Volume 28 Number 9 30 May 2008 ISSN 0278-4343

ELSEVIER

CONTINENTAL SHELF RESEARCH

Research Papers

www.elsevier.com/locate/csr

Continental Shelf Research 28 (2008) 1091–1115

Contents lists available at ScienceDirect

Continental Shelf Research

journal homepage: www.elsevier.com/locate/csr

Saharan dust and phosphatic fidelity: A three-dimensional biogeochemical model of *Trichodesmium* as a nutrient source for red tides on the West Florida Shelf

J.M. Lenes [a,*], B.A. Darrow [a], J.J. Walsh [a], J.M. Prospero [b], R. He [c], R.H. Weisberg [a], G.A. Vargo [a], C.A. Heil [d]

[a] College of Marine Science, University of South Florida, St. Petersburg, FL 33701, USA
[b] Rosenstiel School of Marine and Atmospheric Science, University of Miami, Miami, FL, USA
[c] Department of Marine, Earth & Atmospheric Sciences, North Carolina State University, Raleigh, NC, USA
[d] Fish and Wildlife Research Institute, Florida Fish and Wildlife Commission, St. Petersburg, FL, USA

ARTICLE INFO

Article history:
Received 10 July 2007
Received in revised form
3 December 2007
Accepted 21 February 2008
Available online 5 March 2008

Keywords:
Nitrogen fixation
Modeling
Mineral dust
Iron
Phosphorus
Trichodesmium
Red tide

ABSTRACT

The availability of iron within the surface waters of the broad, oligotrophic West Florida Shelf (WFS) controls periodic blooms of the pelagic marine cyanobacterium *Trichodesmium*. Summer delivery of Saharan dust provided adequate iron (Fe) to shift limitation of growth to the availability of phosphorus (P). Florida's rivers drain Miocene phosphorus deposits to provide the WFS with freshwater nutrient supplies at molar dissolved inorganic nitrogen/phosphate (DIN/PO_4) ratios of <6. These diazotrophs draw upon ubiquitous stocks of dissolved nitrogen gas, once stimulated by Fe-deposition within P-replete waters of the WFS.

An extensive *in situ* data set collected between 1998 and 2001 (NEGOM/ECOHAB) provided plankton taxonomy, hydrographic, nutrient, dissolved organic matter (DOM), pigment, and optical properties on the shelf. We constructed a three-dimensional numerical model to analyze the impact of iron fertilization of the diazotroph *Trichodesmium* and the resultant effect upon the elemental cycles of N, P, and Fe. The coupled physical and ecological models show that the wet deposition of Fe-rich Saharan dust was necessary to stimulate enough nitrogen fixation to initialize the toxic red tide (*Karenia brevis*) of $\sim 20\,\mu g\,chl\,a\,l^{-1}$ that occurred in October 1999. The simulation suggests that the magnitude and longevity of the *Trichodesmium* population, and therefore this source of 'new' nitrogen, was controlled by both phosphorus and iron availability.

1. Introduction

It is a common misconception that nitrogen (N) availability controls production over most of the world's oceans, however, increased awareness of the limiting potential of phosphorus (P) on various time scales has forced a re-investigation of its role (Broecker, 1982; Froelich et al., 1982). Further complicating the issue, the recent IronEx and SOIREE experiments have shown that iron (Fe) is critical in limiting primary production over at least these regions (Martin and Fitzwater, 1988; Barber and Chavez, 1991; Martin et al., 1991; Coale et al., 1996; Gordon et al., 1998; Boyd et al., 2000).

In the oligotrophic West Florida Shelf (WFS) ecosystem (Fig. 1), iron concentrations are extremely low for most of the year (Walsh and Steidinger, 2001; Lenes et al., 2001; Walsh et al., 2006), despite extensive freshwater discharges from the Mississippi River and approximately 25 local rivers along the Florida peninsula. Summer iron concentrations on the WFS are largely controlled by two dominant factors: (1) local riverine inputs (Kim and Martin, 1974; U.S.G.S., 1976–1981) and (2) wind-borne dust transported from Africa (Carder et al., 1991; Prospero, 1999a; Prospero et al., 2001). The high iron content of the West Florida rivers ($>20\,nmol\,kg^{-1}$ at the mouth of Florida Bay; Caccia and Millero, 2003) yields elevated iron concentrations ($1–2\,nmol\,kg^{-1}$ at the 10-m isobath) throughout most summer months (Lenes et al., 2001). However, in the absence of Saharan dust input, mean background iron levels are $<0.1\,nmol\,kg^{-1}$ at the sea surface between the 50- and 200-m isobaths (Fig. 2a, f).

Recent investigations on the WFS food web base suggests a combination of limiting factors (N, P, Fe, Si, temperature, and light) control the seasonal variability of the phytoplankton community and their consequent impact on nutrient cycles (Walsh and Steidinger, 2001; Walsh et al., 2003, 2006). Along the shelf, the toxic red-tide dinoflagellate *Karenia brevis*

* Corresponding author. Tel.: +1 727 553 1112.
E-mail address: lenes@marine.usf.edu (J.M. Lenes).

0278-4343/$ - see front matter © 2008 Elsevier Ltd. All rights reserved.
doi:10.1016/j.csr.2008.02.009

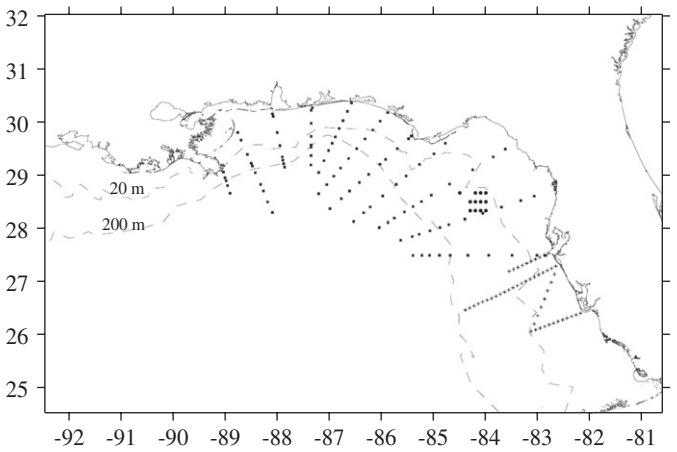

Fig. 1. Location of ECOHAB: Florida (+), ECOHAB middle grounds (●), and NEGOM (■) data sets, relative to the 50 and 200 m isobaths.

forms episodic blooms of $>10\,\mu g$ chl $a\,L^{-1}$ (Walsh and Steidinger, 2001), despite ambient nitrate (NO_3) concentrations of $<0.50\,\mu mol\,N\,kg^{-1}$ within 5 km of the Florida coast (Steidinger et al., 1998). Offshore, background NO_3 concentrations are $<0.05\,\mu mol\,N\,kg^{-1}$ (Masserini and Fanning, 2000).

Therefore, an additional source of 'new' nitrogen is needed to support the elevated red tide biomass that is usually first observed near shore between Tampa Bay and Charlotte Harbor (Walsh et al., 2006). At 18–25 °C, thermal impacts on gas solubility suggest a change in dinitrogen stocks of 383–429 $\mu mol\,N_2\,kg^{-1}$ (Weiss, 1970) at the same salinity of 35.0 within surface waters of the WFS. Thus, one possible source of 'new' nitrogen, nitrogen fixation by the colonial diazotroph *Trichodesmium erythraeum* appears to play an important role in the nitrogen economy of *K. brevis* along the WFS (Walsh and Steidinger, 2001). Blooms of *T. erythraeum* have been observed within 75 km of the west coast of Florida for more than 50 yr (King, 1950), while surface stocks of these diazotrophs have reached $>200\,\mu g$ chl $a\,l^{-1}$, as found off St. Pete Beach during May 2000 (Walsh et al., 2006).

The examination of the factors controlling *Trichodesmium* growth indicate potential limitation by both Fe (Berman-Frank et al., 2001; Lenes et al., 2001; Orcutt et al., 2001) and phosphorus supplies (Karl et al., 1997; Sanudo-Wilhelmy et al., 2001; Mills et al., 2004; Lenes et al., 2005). For example, Orcutt et al. (2001) found a variable Fe/N ratio (1.9×10^{-4}–2.9×10^{-3}) dependent upon iron availability, implying a direct effect on cell health. While phosphorus limitation was reported for *Trichodesmium* populations at the Bermuda Atlantic Time Series (BATS) site (Sanudo-Wilhelmy et al., 2001) and the Hawaii Ocean Time-Series (HOTS) station (Karl et al., 1997).

Prospero (1999b) recently showed from a 23 yr aerosol record at Miami that large amounts of aeolian mineral dust are periodically carried into Florida every summer yielding daily atmospheric concentrations from 10 to $100\,\mu g\,m^{-3}$ above Miami (Fig. 3). Maximum concentrations of this Saharan dust occur between June and August (Prospero et al., 2001). Landing et al. (1995) measured mineral dust deposition rates ranging from 0.78 to $1.9\,g\,m^{-2}\,yr^{-1}$ across the length of Florida. Dust deposition is highly episodic with as much as 80% of the annual deposition occurring in one summer month (Lenes et al., 2001). Similarly, Prospero et al. (1987) reported a deposition of $1.3\,g\,m^{-2}$ in a 1-yr study in Miami, falling in the middle of Landing's range of values. The long-term importance of African dust to biogeochemical processes in the Florida region is evidenced by the fact that non-calcareous soils in the state are largely comprised of African dust (Muhs et al., 2007).

During the 5–7 July 1999 ECOHAB (Ecology and Oceanography of Harmful Algal Blooms) cruise, after a 26 June–4 July Saharan dust event, we measured a mean of $3.0\,nmol\,Fe\,kg^{-1}$ in near-surface waters at salinities >35.0 (stations above the 50–200 m isobaths) remote from riverine inputs (Fig. 2). In contrast, on the WFS during the August 1998, May 1999, and May 2000 cruises, in the absence of Saharan dust input, Fe concentrations were at background levels of $<0.3\,nmol\,kg^{-1}$ (Lenes et al., 2001).

Summer atmospheric delivery of Fe, in the form of Saharan dust, thus increased surface dissolved Fe concentrations 3–30 times over background levels, with a subsequent 100-fold increase of *Trichodesmium* stocks at mid-shelf during 1999 (Lenes et al., 2001). A concurrent depletion of mid-shelf stocks of inorganic and organic phosphorus between June and July 1999 (Fig. 4) suggests that the potential size of the diazotroph bloom during the dust season may be regulated by P-limitation within the offshore system as well. Ridame and Guieu (2002) calculated that aeolian input of phosphorus could play a significant role in the oligotrophic western Mediterranean Sea. Based on their calculations of P-input relative to dust concentration, this P source would be negligible (nM) relative to P concentrations measured on the WFS (μM).

The near-shore estuarine supplies of nutrients along the West Florida coast yield low molar N/P ratios (Walsh et al., 2003). These coastal waters intersect with offshore subsurface populations of *Trichodesmium* (Walsh et al., 2006), in response to shoreward transport of near-bottom mid-shelf waters during wind-driven circulation events of local upwelling. Dissolved inorganic nitrogen (DIN) to phosphate (PO_4) ratios of <6 within the Caloosahatchee River, Charlotte Harbor, Sarasota and Tampa Bays emphasize the importance of the fossil Hawthorne formation (Dragovich and Kelly, 1968) in nutrient loading from the southern estuaries. In contrast, the DIN/PO_4 ratios are >40 for the nutrient supplies of the northern estuaries and ~16 for deep-sea intrusions on the shelf (Walsh et al., 2006). Since the molar N:P ratio of fertilizers reaching drainage basins of the Gulf of Mexico are ~8 (Turner and Rabalais, 1994), the remaining phosphorus found in the central west Florida region could be attributed to both fossil phosphorus (Dragovich and Kelly, 1968) and agricultural phosphorus sources.

Measurements of the molar DIN/PO_4 ratios in the eastern Gulf of Mexico during May 1999 were >15 over most of the northern shelf and <15 south of the Big Bend region and on the outer shelf (Fig. 5a, b). These WFS DIN and PO_4 concentrations in spring 1999 reflected prior nutrient loadings supplied to each part of the shelf by the different river systems (Walsh et al., 2006). By August 1999, the DIN/PO_4 ratios had increased along the outer and mid-shelf regions south of the Big Bend (Fig. 5c). Since little change in phosphate was observed, an additional source of nitrogen must have led to the elevation in the DIN/PO_4 ratios.

Diazotrophs are sources of ammonium during both the population growth phase (Prufert-Bebout et al., 1993) and after bloom collapse (Devassy et al., 1978). In addition, studies have shown that up to 50% of the N_2 fixed by *Trichodesmium* can be excreted as DON, with 50–100% released as amino acids (Capone et al., 1994; Glibert and Bronk, 1994) and ammonium (Mulholland and Capone, 2000). Mulholland et al. (2004, 2006) found that *K. brevis* grows with increased concentrations of both NH_4 and DON derived from continuous cultures of *Trichodesmium*. Thus, our simulation analysis explored the hypothesis that large pools of N derived from diazotrophic origins will accumulate in the WFS water column during periods of Fe-availability on the outer shelf thereby mitigating nitrogen limitation in other phytoplankton communities and the microbial loop. The intent of this study was to test this hypothesis first posed by Lenes et al. (2001).

High concentrations of organic N and P had been measured at the beginning of *K. brevis* blooms, but the nutrients could not be

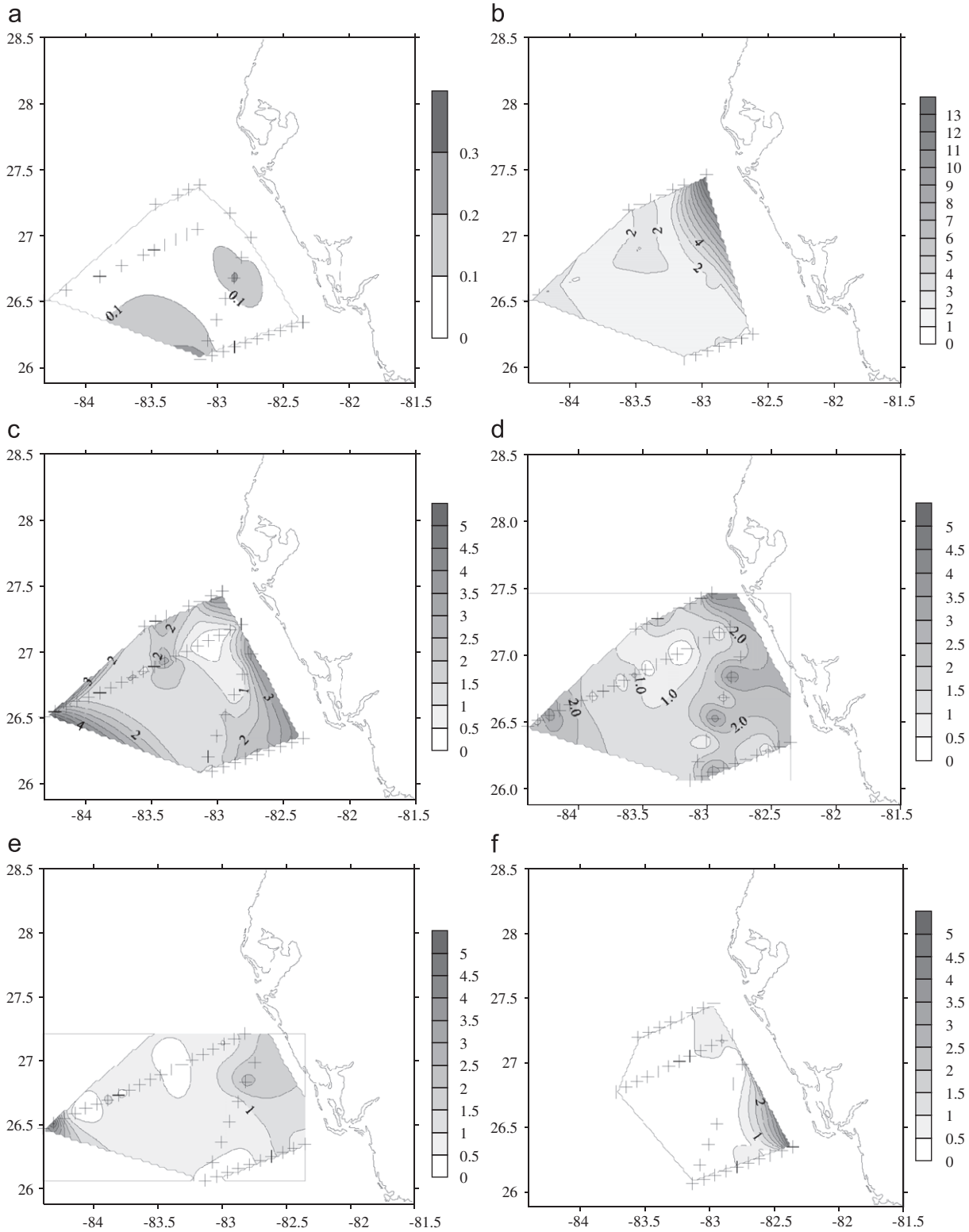

Fig. 2. The 1999 surface distributions of total dissolved iron (nmol kg^{-1}) across the West Florida Shelf during (a) 2–5 May, (b) 5–8 June, (c) 5–7 July, (d) 6–8 August, (e) 7–9 September, and (f) 5–7 October.

linked to estuarine sources (Lester et al., 2001). During 1999, *Trichodesmium* populations increased two orders of magnitude above background levels, leading to elevated DON concentrations of ~7 to ~15 μmol kg^{-1} within the peak *Trichodesmium* population (Fig. 6). This amount of 'new' nitrogen could yield a red tide of >20 μg chl $a\,l^{-1}$ of the toxic dinoflagellate *K. brevis* (Walsh and Steidinger, 2001).

Previous models have had some success in analyzing the role of *Trichodesmium* in open ocean nutrient dynamics (Hood et al., 2001, 2004; Fennel et al., 2002; Moore et al., 2002; Lenes et al.,

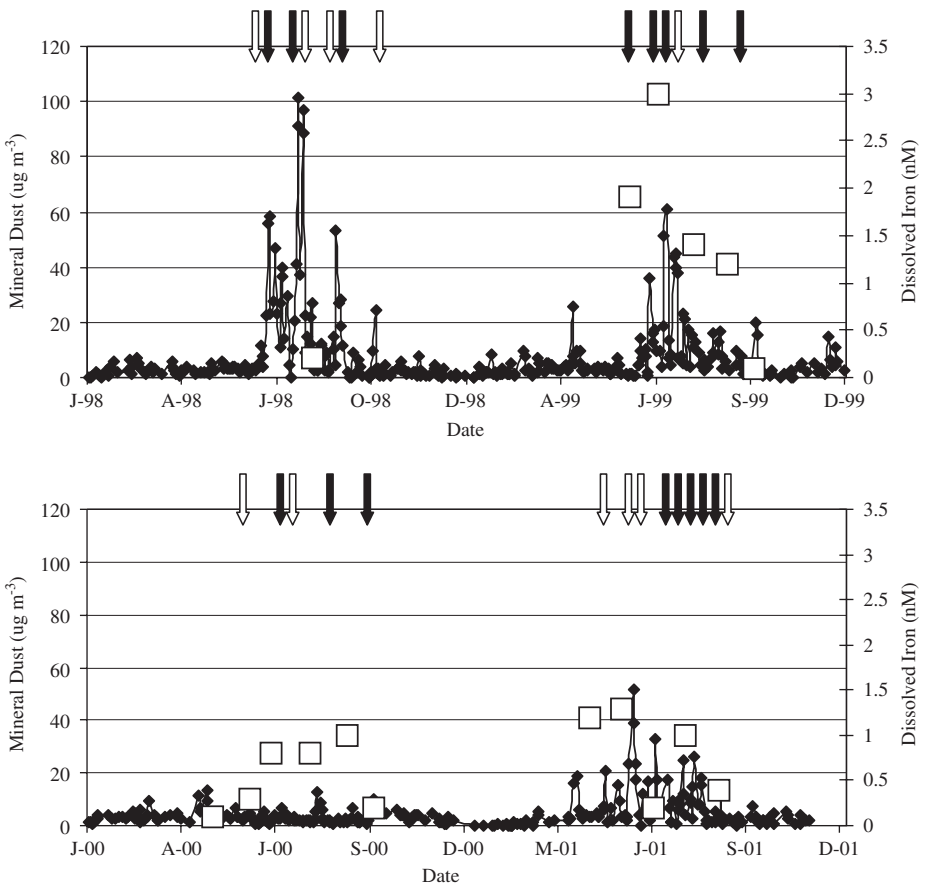

Fig. 3. Mineral dust concentration (solid line) at Miami from 1998–2001 in relation to the offshore surface dissolved iron concentration (hollow squares) on the West Florida Shelf averaged between the 50 and 200 m isobaths. Saharan dust events of low nss-nitrate are denoted by arrows, with filled arrows indicating concurrent wet deposition (i.e., 24–48 h delay) at the Tampa Airport of >1.0 mm rain.

2005). However, there are no *Trichodesmium*-based models that analyze nitrogen fixation as a nutrient source for coastal red tide events. While these models employ similarly complex formulations, they focus on large scale, open-ocean estimates. We attempt to incorporate a multivariable analysis of a fine grid, coastal simulation to investigate the role of each parameter on the overall success of *Trichodesmium*. Here we present a three-dimensional, time-dependent biophysical simulation model that incorporates the variables that could play a role in the development of coastal *Trichodesmium* populations: iron, phosphorus, vertical migration, cell death, and the vertical and horizontal transport in a three-dimensional shelf environment (Weisberg and He, 2003).

2. Methods

The coupled three-dimensional model is composed of four submodels: (1) physical (water circulation), (2) bio-optical [see Appendix A], (3) atmospheric (dust input), and (4) biochemical [see Appendix B]. The solutions of 24 partial differential equations described the spatio-temporal fields of: temperature, salinity, u, v, w, k_z, spectral light, atmospheric dust, diatoms (P_1), *Trichodesmium* (P_2), ammonifying bacteria (B_1), nitrifying bacteria (B_2), dissolved iron (dFe), colloidal iron (cFe), dissolved organic carbon (DOC), dissolved organic nitrogen (DON), dissolved organic phosphorus (DOP), dissolved inorganic carbon (DIC), nitrate+nitrite (NO_3), ammonia (NH_4), phosphate (PO_4), siliceous detritus (D_1), non-siliceous detritus (D_2), and siliceous fecal pellets (Z_1). Subject to estuarine and shelf-break boundary conditions, they were solved over an orthogonal curvilinear grid (Fig. 7) of the WFS at a horizontal resolution of ~2–6 km, with 21 vertical sigma levels (He and Weisberg, 2002a, b, 2003). Two distinct cases were run (with and without aeolian dust) to test the significance of atmospherically derived iron.

2.1. Physical model-equations of motion

The advective transport (Tr_a) term was described by

$$Tr(\mathrm{d}A)_a = -\frac{[(\partial/\partial\xi)(h_2 u\,\mathrm{d}A) + (\partial/\partial\zeta)(h_1 v\,\mathrm{d}A) + h_1 h_2(\partial/\partial\sigma)(\omega A)]}{h_1 h_2} \quad (1)$$

where A was any of the above state variables to which the transport applied, ξ was the horizontal curvilinear coordinate in the cross-shelf direction, ζ was the horizontal curvilinear coordinate in the alongshelf direction, h_1 and h_2 were the length and width of the grid cell in the x and y direction respectively, and u, v and ω were the velocities in the x, y, and z directions from the circulation model (Table 1). Due to the strong horizontal diffusion in the numerical algorithm for advective transport, explicit horizontal turbulent mixing was ignored and modeled only in the vertical component, such that diffusive transport (Tr_d) was

$$Tr(\mathrm{d}A)_d = \frac{\partial}{\partial\sigma}\left(\frac{k_h}{d}\frac{\partial A}{\partial\sigma}\right) \quad (1a)$$

where k_h was the coefficient of vertical eddy diffusivity, derived from a second momentum turbulence closure scheme, embedded within the Princeton Ocean Model (POM) (Mellor and Yamada, 1982).

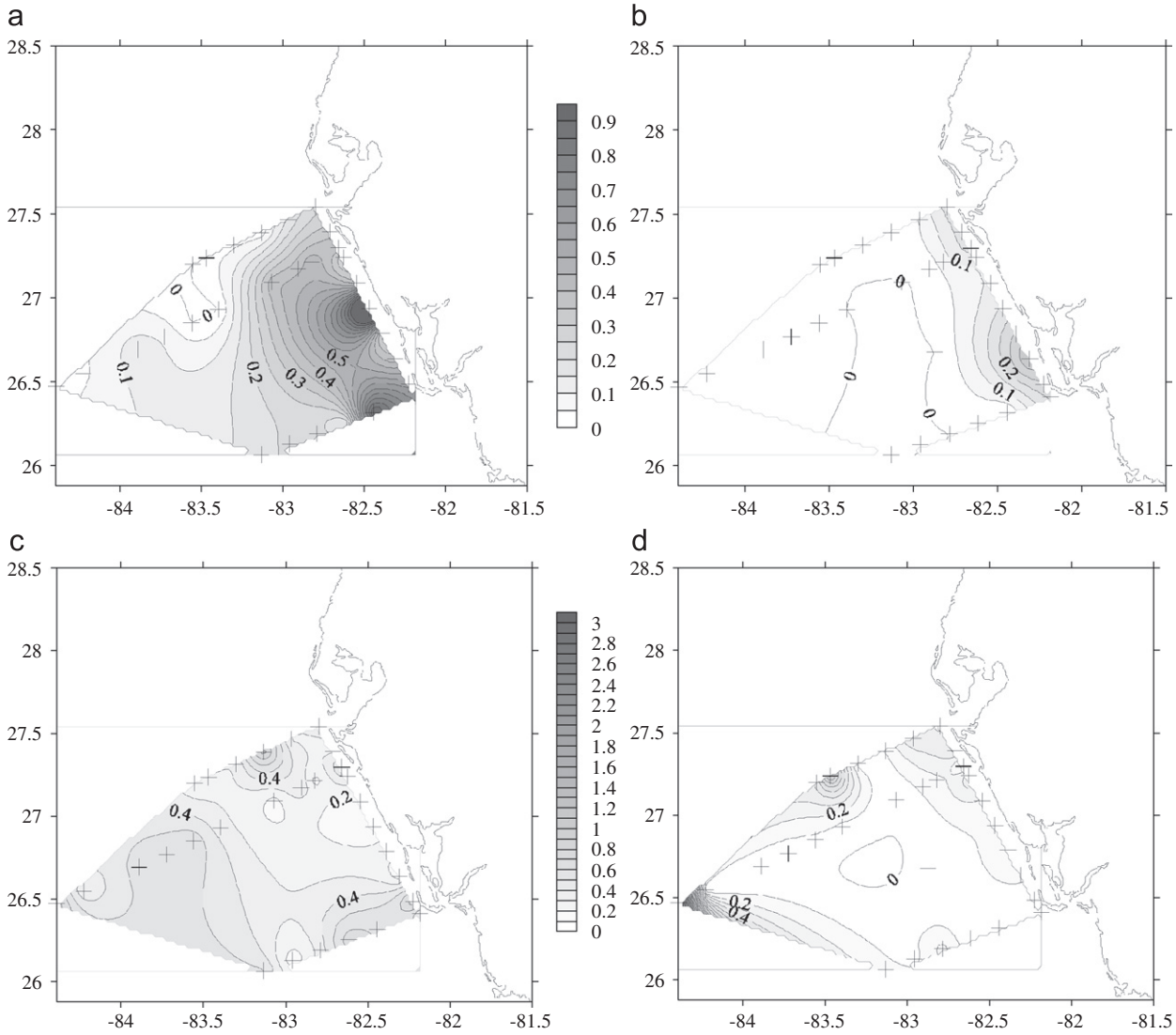

Fig. 4. The 1999 surface distributions of phosphate and dissolved organic phosphorus (μmol kg^{-1}) across the West Florida Shelf during (a, c) 5–8 June and (b, d) 5–7 July.

2.2. Bio-optics

A simple spectral solar irradiance model (Gregg and Carder, 1990) was employed to derive solar irradiance at 30 visible spectral wavelengths (10 nm intervals) below the ocean surface ($I_{0(\lambda)}$) [see Appendix A]. In the marine environment, several variables influence the intensity and spectral quality of light. Light energy is absorbed and scattered by the water, the organic component, i.e. algae, colored dissolved organic matter (Kirk, 1994), bacteria (Nelson and Robertson, 1993), and the non-living particulate matter, i.e. detritus. The underwater light field not only determines the photosynthetic efficiency of the photoautotrophs, but the position of *Trichodesmium* in the water column due to buoyancy regulation in relation to the ambient light field (Kromkamp and Walsby, 1992).

2.3. Dust deposition

The deposition of dust aerosols required several parameterizations to simulate concentrations within the surface mixed layer of the ocean. Gravitational sedimentation, turbulent mixing, and wet deposition by rain all greatly affect the fallout of dust, with varying importance based on precipitation rates and particle size (Tegen and Fung, 1994). We developed a two-dimensional atmospheric deposition model to provide daily dust estimates as a source for Fe fertilization (Lenes, 2006). Aerosols collected at Ft. Myers in 1995 and 1996 showed similar concentrations at almost no lag time when compared with the Miami data (Prospero et al., 2001). Therefore, atmospheric concentrations of dust aerosols collected at Miami represented concentrations over the WFS during 1999 (Fig. 3).

2.4. Iron

The biological and chemical interactions that determine iron cycling in marine systems are poorly understood. Several assumptions were made in order to simulate water column concentrations [see Appendix B]. Sources include atmospheric input, riverine outflow, and sediment resuspension, while losses are derived from biological uptake, organic complexation, precipitation as iron oxides, and particulate scavenging. These loss terms represent removal from the dissolved pool, but are still available for remineralization and photoreduction in the model.

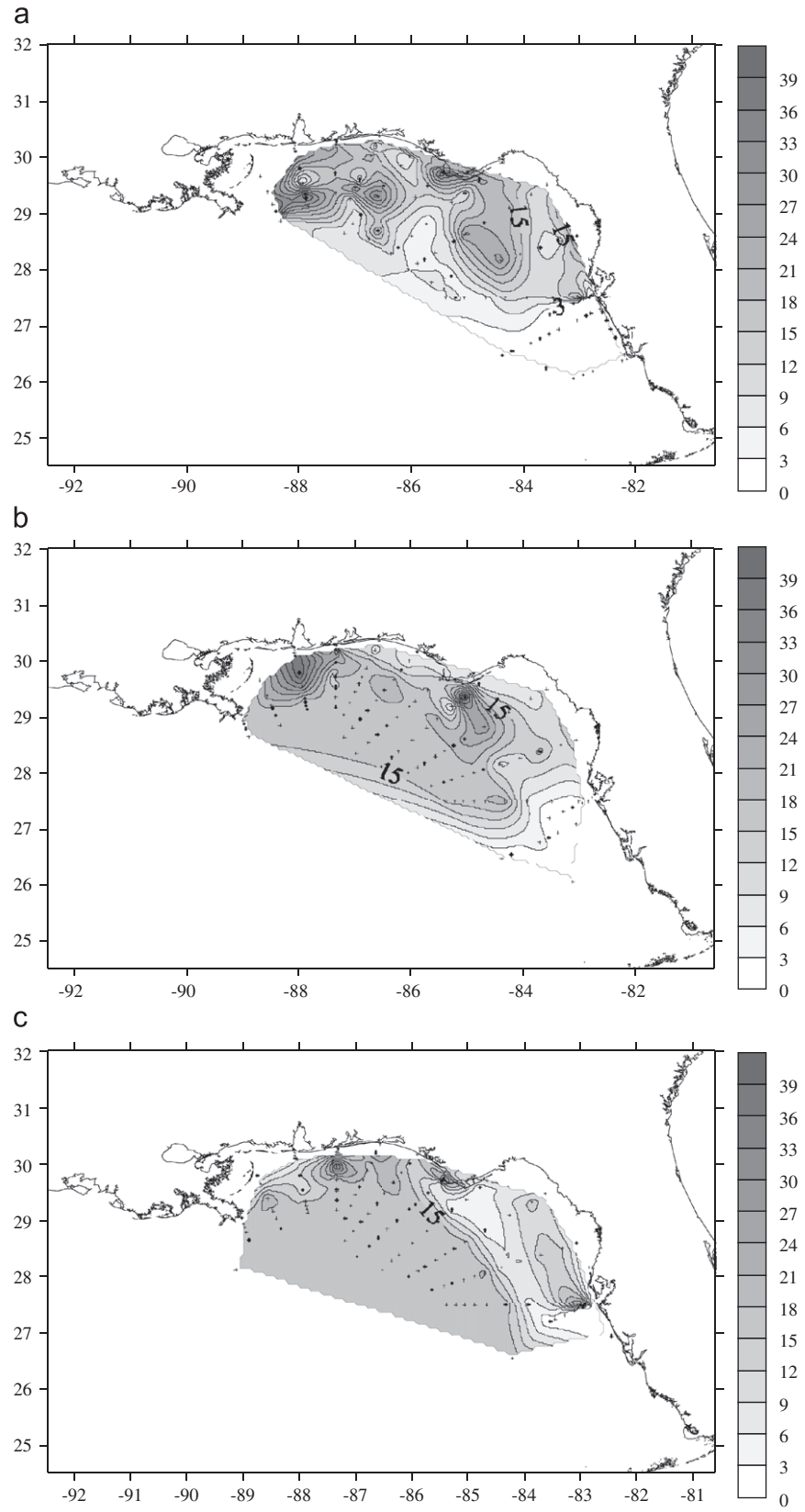

Fig. 5. The molar DIN/PO_4 ratios (mol/mol) in the eastern Gulf of Mexico at the (a) surface and (b) bottom in May 1999, and (c) at the bottom in August 1999.

In an attempt to simplify non-atmospheric iron sources, riverine supplies were accounted for using boundary conditions. A salinity to iron ratio was determined for near shore grid points ($\leqslant$4 m depth):

$$dFe = -0.0002sal + 0.0074 \quad (2)$$

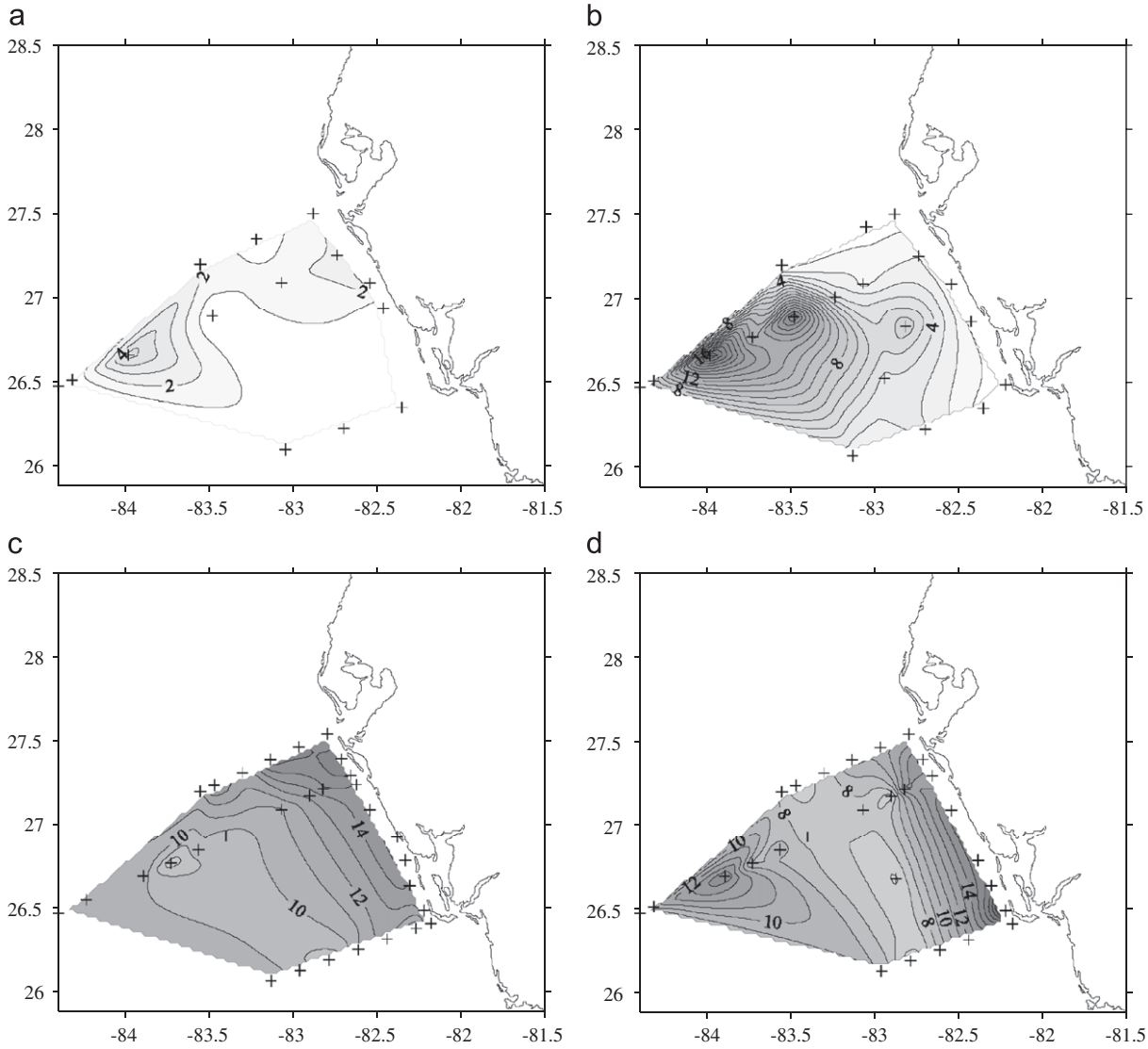

Fig. 6. The 1999 surface distributions of *Trichodesmium* (colonies l^{-1}) and dissolved organic nitrogen (μmol kg^{-1}) across the West Florida Shelf during (a, c) 2–5 May and (b, d) 5–7 July, as sampled by bottles.

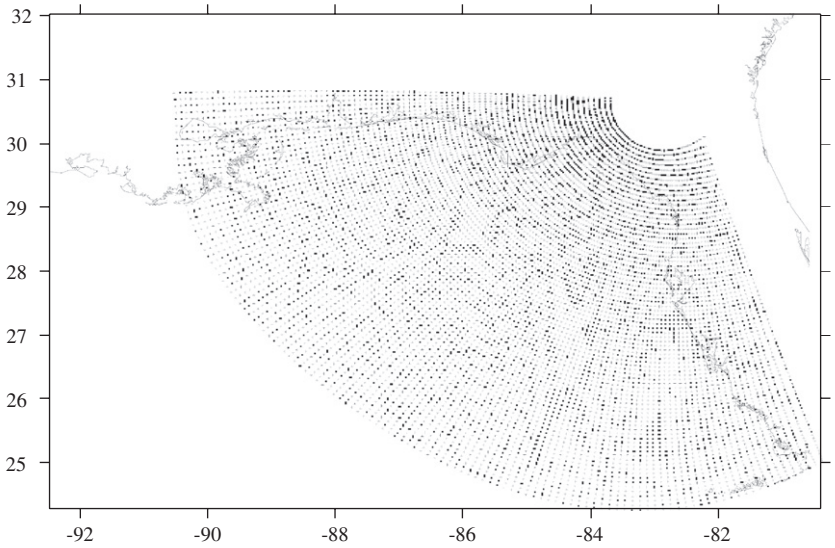

Fig. 7. The orthogonal curvilinear grid at a resolution of ~2–6 km.

Table 1
Symbol description and values

Symbol	Description	Units	Value
b	Rate of phototransformation of DOM to inorganic matter	s^{-1}	1.98E−9
B	Total bacteria	$mmol\,m^{-3}$	–
B_1	Ammonifying bacteria	$mmol\,m^{-3}$	–
B_2	Nitrifying bacteria	$mmol\,m^{-3}$	–
cFe	Concentration of colloidal iron	$\mu mol\,m^{-3}$	–
CDOM	Colored dissolved organic matter	$mmol\,m^{-3}$	–
d	Depth of sigma level	m	–
dFe	Concentration of dissolved iron	$\mu mol\,m^{-3}$	–
dFe_i	Iron input into the upper sigma level	$\mu mol\,m^{-3}$	–
D	Total detritus	$mmol\,m^{-3}$	–
D_1	Diatom detritus	$mmol\,m^{-3}$	–
D_2	*Trichodesmium* detritus	$mmol\,m^{-3}$	–
DIC	Concentration of dissolved inorganic carbon	$mmol\,m^{-3}$	–
DOC	Concentration of dissolved organic carbon	$mmol\,m^{-3}$	–
DON	Concentration of dissolved organic nitrogen	$mmol\,m^{-3}$	–
DOP	Concentration of dissolved organic phosphorus	$mmol\,m^{-3}$	–
F	Molecular weight of iron	$g\,mole^{-1}$	55.847
Fe_m	Mass fraction of iron in mineral aerosols	%	3.5
Fe_d	Iron dissolution rate	%	5.0
h_1	Transformation coefficient from the Cartesian (x) to the orthogonal (ξ)	–	–
h_2	Transformation coefficient from the Cartesian (y) to the orthogonal (ζ)	–	–
$I_{0(\lambda)}$	Solar irradiance at wavelength, λ, just below the ocean surface	$\mu E\,m^{-2}\,s^{-1}$	–
I_0	Saturation intensity effecting photoreduction of colloidal iron	$\mu E\,m^{-2}\,s^{-1}$	2500
$I_{sat(1)}$	Saturation intensity effecting growth for diatoms	$\mu E\,m^{-2}\,s^{-1}$	250
$I_{sat(2)}$	Saturation intensity effecting growth for a *Trichodesmium*	$\mu E\,m^{-2}\,s^{-1}$	400
I_z	Total incident radiation at depth, z, over all wavelengths (400–700 nm)	$\mu E\,m^{-2}\,s^{-1}$	–
$I_{z(\lambda)}$	Incident radiation at depth, z, and wavelength, λ	$\mu E\,m^{-2}\,s^{-1}$	–
k_{scFe}	Half-saturation constant for iron scavenging by particles	$\mu mol\,m^{-3}$	1.5
$k_{B(\lambda)}$	Specific attenuation coefficient of bacteria at wavelength, λ	M^{-1}	–
$k_{C(\lambda)}$	Specific attenuation coefficient of CDOM at wavelength, λ	m^{-1}	–
k_d	Detritus remineralization rate	s^{-1}	5.7E−7
$k_{dFe(1)}$	Half-saturation constant for dFe uptake for diatoms	$\mu mol\,m^{-3}$	0.2
$k_{dFe(2)}$	Half-saturation constant for dFe uptake for *Trichodesmium*	$\mu mol\,m^{-3}$	0.5
$k_{DOC(3)}$	Half-saturation constant for DOC uptake for ammonifying bacteria	$mmol\,m^{-3}$	45
$k_{DON(3)}$	Half-saturation constant for DON uptake for ammonifying bacteria	$mmol\,m^{-3}$	6.5
$k_{DOP(2)}$	Half-saturation constant for DOP uptake for *Trichodesmium*	$mmol\,m^{-3}$	0.2
$k_{DOP(3)}$	Half-saturation constant for DOP uptake for ammonifying bacteria	$mmol\,m^{-3}$	0.25
k_{fp}	Fecal pellet remineralization rate	s^{-1}	5.7E−7
k_h	Coefficient of vertical eddy diffusivity	$cm\,s^{-1}$	–
k_{hvC}	Rate constant for photoreduction of colloidal iron	s^{-1}	2.33E−4
$k_{NH4(1)}$	Half-saturation constant for ammonia uptake for diatoms	$mmol\,m^{-3}$	1.5
$k_{NH4(4)}$	Half-saturation constant for ammonia uptake for nitrifying bacteria	$mmol\,m^{-3}$	0.2
$k_{NO3(1)}$	Half-saturation constant for nitrate uptake for diatoms	$mmol\,m^{-3}$	1.0
$k_{P1(\lambda)}$	Specific attenuation coefficient of diatoms at wavelength, λ	m^{-1}	–
$k_{P2(\lambda)}$	Specific attenuation coefficient of *Trichodesmium* at wavelength, λ	m^{-1}	–
k_{photo}	Rate of photoreduction of colloidal iron	$\mu mol\,m^{-3}\,s^{-1}$	–
$k_{PO4(1)}$	Half-saturation constant for phosphate uptake for diatoms	$mmol\,m^{-3}$	0.1
$k_{PO4(2)}$	Half-saturation constant for phosphate uptake for *Trichodesmium*	$mmol\,m^{-3}$	0.1
$k_{PO4(4)}$	Half-saturation constant for phosphate uptake for nitrifying bacteria	$mmol\,m^{-3}$	0.05
$k_{w(\lambda)}$	Specific attenuation coefficient of water at wavelength, λ	m^{-1}	–
k_λ	Total attenuation coefficient at wavelength, λ	m^{-1}	–
k_{zoo}	Maximum grazing rate on diatoms	$mmol\,m^{-3}\,s^{-1}$	1.15E−5
M_3	Ammonifying bacterial mortality	s^{-1}	2.77E−6
M_4	Nitrifying bacterial mortality	s^{-1}	2.77E−6
NH_4	Concentration of ammonium	$mmol\,m^{-3}$	–
NO_3	Concentration of nitrate+nitrite	$mmol\,m^{-3}$	–
pCO_2	CO_2 concentration in water	$Mmol\,m^{-3}$	–
pCO_{2air}	CO_2 concentration in air	μatm	383
P_1	Concentration of diatoms	$mmol\,m^{-3}$	–
P_2	Concentration of *Trichodesmium*	$mmol\,m^{-3}$	–
PO_4	Concentration of inorganic phosphate	$mmol\,m^{-3}$	–
$P^{ref}_{(1)}$	Background population for diatoms	$mmol\,m^{-3}$	0.5
$P^{ref}_{(2)}$	Background population for *Trichodesmium*	$mmol\,m^{-3}$	0.01
r_1	Coefficient for diatom grazer respiration	–	0.2
r_2	Coefficient for *Trichodesmium* grazer respiration	–	0.2
r_3	Ingestion coefficient for grazing on diatoms	–	0.8
r_4	Ingestion coefficient for grazing on *Trichodesmium*	–	0.8
T	Time step	s	360
T	Temperature	°C	–
TDP	Total dissolved phosphorus	$mmol\,m^{-3}$	–
Tr_a	Transport due to advection	$cm\,s^{-1}$	–
Tr_b	Transport due to diffusion	$cm\,s^{-1}$	–
Tr_t	Total transport	$cm\,s^{-1}$	–
U	Velocity in the ξ direction	$cm\,s^{-1}$	–
V	Velocity in the ζ direction	$cm\,s^{-1}$	–

Table 1 (*continued*)

Symbol	Description	Units	Value
W_1	Sinking rate of diatoms	$m\,s^{-1}$	5.7E–6
W_2	Vertical migration rate of *Trichodesmium*	$mm\,s^{-1}$	± 0.9
X	Rate of dFe loss to higher trophic levels	s^{-1}	8.68E–5
Z	Depth interval within the water-column	M	–
Z_1	Diatomaceous fecal pellets	$mmol\,m^{-3}$	–
α	Particle scavenging of iron	s^{-1}	–
χ_1	Diatom lysis rate	%	3.0
χ_2	*Trichodesmium* lysis rate	$mmol\,m^{-3}\,s^{-1}$	–
ε_1	Diatom respiration rate	%	10.0
ε_2	*Trichodesmium* respiration rate	%	12.0
ε_3	Ammonifying bacteria respiration rate	%	45.0
ε_4	Nitrifying bacteria respiration rate	%	45.0
ϕ_1	Wet deposition of mineral aerosols	$\mu g\,m^{-3}\,d^{-1}$	–
ϕ_2	Dry deposition of mineral aerosols	$\mu g\,m^{-3}\,d^{-1}$	–
γ_1	Diatom grazing rate	$mmol\,m^{-3}\,s^{-1}$	–
γ_2	*Trichodesmium* grazing rate	%	1.0
λ	Wavelength of radiation	nm	–
μ_1	Realized net growth rate for diatoms	s^{-1}	–
μ_2	Realized net growth rate for *Trichodesmium*	s^{-1}	–
μ_3	Realized net growth rate for ammonifying bacteria	s^{-1}	–
μ_4	Realized net growth rate for nitrifying bacteria	s^{-1}	–
μ_{max1}	Maximum gross growth rate for diatoms	s^{-1}	1.45E–5
μ_{max2}	Maximum gross growth rate for *Trichodesmium*	s^{-1}	8.1E–6
μ_{max3}	Maximum gross growth rate for ammonifying bacteria	s^{-1}	1.5E–5
μ_{max4}	Maximum gross growth rate for nitrifying bacteria	s^{-1}	1.5E–5
μ^T_{max1}	Maximum gross growth rate for diatoms adjusted for temp.	s^{-1}	–
μ^T_{max2}	Maximum gross growth rate for *Trichodesmium* adjusted for temp.	s^{-1}	–
σ	Sigma coordinate	–	–
υ_1	Fraction of maximum nutrient uptake by diatoms	$mmol\,m^{-3}$	–
υ_2	Fraction of maximum nutrient uptake by *Trichodesmium*	$mmol\,m^{-3}$	–
υ_3	Fraction of maximum nutrient uptake by ammonifying bacteria	$mmol\,m^{-3}$	–
υ_4	Fraction of maximum nutrient uptake by nitrifying bacteria	$mmol\,m^{-3}$	–
ω	Velocity component in the σ direction	$cm\,s^{-1}$	–
ξ	Cross-shelf curvilinear coordinates	–	–
ψ_1	Excretion rate of diatoms	%	4·0
ψ_2	Excretion rate of *Trichodesmium*	%	25.0
ζ	Alongshore curvilinear coordinates	–	–

over the salinity range 22–34 {sal > 34, dFe = 0.0004; sal < 22, dFe = 0.003}, allowing for increased iron concentrations during periods of increased river outflow. This boundary equation was regressed from measurements of total dissolved iron (Lenes et al., 2001) collected near shore during ECOHAB:Florida (1998–2001). Remineralization of particulate organic iron in the bottom sigma layer served as the bottom boundary source.

2.5. Boundary and initial conditions

We utilized monthly data collected during cross-shelf sections off Tampa Bay, Sarasota, and Charlotte Harbor during March 1998–November 2001 (Fig. 1) as part of the NOAA/EPA ECOHAB: Florida study. During these studies, we obtained temperature, salinity, nutrients (NO_3, NO_2, NH_4, PO_4, Fe, DOP, and DON), chlorophyll *a*, phaeopigmnents, PON, POC, POP, and abundances of the dominant phytoplankton species. Similar measurements were collected during 2001–2002 as part of the NSF-funded program DOTGOM.

Additionally, surface seawater samples were collected at discrete optical stations and processed for absorption spectra by total particles ($a_p(\lambda)$), detritus ($a_d(\lambda)$), and colored dissolved organic matter (CDOM) ($a_{CDOM}(\lambda)$). Quarterly surveys of the MMS NEGOM [Northeastern Gulf of Mexico] Project (http://www.gomr.mms.gov) provided the data across 11 other sections during spring, summer, and fall of 1998–2000 (Fig. 1). This third set of observations includes ADCP, salinity, temperature, chlorophyll, CDOM data, and discrete observations of nutrients (NO_3, NO_2, NH_4, urea, PO_4), HPLC pigments, POC, PON, turbidity, and the same bioptical properties. These data sets provided initial (Table 2) and open boundary [western boundary] (Table 3) conditions for the biochemical model [see Appendix B] predictions of the availability of nutrients to primary producers via both deep-sea and fluvial supplies. Nutrient and chlorophyll ratios varied for each functional group (Table 4).

Finally, salinity-to-nutrient ratios were set for near-shore grid points ($\leqslant 4$ m) to mimic riverine input using the same formulation as for dFe (Eq. (2)). We calculated PO_4 between salinities of 22–34 {sal > 34, $PO_4 = 0.025$; sal < 22, $PO_4 = 1.225$}:

$$PO_4 = -0.1sal + 3.425 \quad (3)$$

for all coastal boundaries. Variations in molar N:P ratios had been measured along the coast (16–30 for northern rivers; 2–6 for southern rivers; Walsh et al., 2006). In order to simulate this pattern, we added inorganic nutrients at a NO_3/PO_4 ratio of ~20 north of 28.5°N latitude and ~3 south of 28.5°N latitude. DIC was 2100 μmol kg^{-1} at the river boundaries.

In the model, the *Trichodesmium* population was reported as a depth-integrated biomass (mg chl $a\,m^{-2}$) despite validation data measured at the surface in concentration units (colonies l^{-1}). This gave a more consistent representation of the model behavior with respect to *Trichodesmium* biomass due to changes in its vertical position within the water column by calculated vertical migration.

Table 2
Initial conditions applied uniformly over the West Florida shelf

Depth (m)	P_1 (mmol C m^{-3})	P_2 (mmol C m^{-3})	NH_4 (mmol m^{-3})	NO_3 (mmol m^{-3})	PO_4 (mmol m^{-3})	DON (mmol m^{-3})	DOP (mmol m^{-3})	DOC (mmol m^{-3})
1	0.125	0.02	0.1	0.05	0.05	6.5	0.1	55
10	0.125	0.02	0.1	0.05	0.05	6.5	0.1	55
50	0.125	0.02	0.1	0.05	0.05	6.5	0.1	55
100	0.125	0.01	0.1	0.05	0.05	6.5	0.1	55
150	0.125	0	0.1	0.05	0.05	6.2	0.1	54
200	0	0	0.1	5.04	0.24	6	0.1	53
250	0	0	0.1	7.55	0.375	6	0.1	52
300	0	0	0.1	9.06	0.5	6	0.1	51
350	0	0	0.1	10.57	0.595	6	0.1	50
400	0	0	0.1	12.08	0.68	6	0.1	49
450	0	0	0.1	13.59	0.765	6	0.1	48
500	0	0	0.1	15.1	0.85	6	0.1	47
600	0	0	0.1	18.12	1.02	6	0.1	46
700	0	0	0.1	21.14	1.19	6	0.1	45
800	0	0	0.1	24.16	1.36	6	0.1	45
900	0	0	0.1	27.18	1.53	6	0.1	45
1000	0	0	0.1	27.5	1.75	6	0.1	45
1500	0	0	0.1	30	1.75	6	0.1	45
2000	0	0	0.1	35	1.75	6	0.1	45
2500	0	0	0.1	40	1.75	6	0.1	45

Depth (m)	DIC (mmol m^{-3})	Z_1 (mmol C m^{-3})	B_1 (mmol C m^{-3})	B_2 (mmol C m^{-3})	D_1 (mmol C m^{-3})	D_2 (mmol C m^{-3})	dFe (mmol m^{-3})	cFe (mmol m^{-3})
1	2100	0	0.05	0.05	0.005	0.005	0.0003	0.0003
10	2100	0	0.05	0.05	0.005	0.005	0.0003	0.0003
50	2100	0	0.05	0.05	0.005	0.005	0.0003	0.0003
100	2100	0	0.05	0.05	0.005	0.005	0.0003	0.0003
150	2100	0	0.05	0.05	0.005	0.005	0.0004	0.0004
200	2120	0	0.05	0.05	0.005	0.005	0.0005	0.0005
250	2125	0	0.05	0.05	0.005	0.005	0.0005	0.0005
300	2130	0	0.05	0.05	0.005	0.005	0.0005	0.0005
350	2135	0	0.05	0.05	0.005	0.005	0.0006	0.0006
400	2140	0	0.05	0.05	0.005	0.005	0.0006	0.0006
450	2145	0	0.05	0.05	0.005	0.005	0.0006	0.0006
500	2150	0	0.05	0.05	0.005	0.005	0.0007	0.0007
600	2160	0	0.05	0.05	0.005	0.005	0.0007	0.0007
700	2170	0	0.05	0.05	0.005	0.005	0.0008	0.0008
800	2180	0	0.05	0.05	0.005	0.005	0.0008	0.0008
900	2190	0	0.05	0.05	0.005	0.005	0.0009	0.0009
1000	2200	0	0.05	0.05	0.005	0.005	0.0009	0.0009
1500	2200	0	0.05	0.05	0.005	0.005	0.001	0.001
2000	2200	0	0.05	0.05	0.005	0.005	0.001	0.001
2500	2200	0	0.05	0.05	0.005	0.005	0.001	0.001

3. Results and discussion

3.1. *Trichodesmium*

On 4 May 1999, the model yields a depth-integrated *Trichodesmium* chlorophyll biomass maximum along the outer WFS (Fig. 8a). Bottom nitrate (Fig. 8b) and phosphate (Fig. 8c) concentrations were low compared with 1998 when anomalously strong winds from the west forced deep-sea water through the DeSoto Canyon at the northeastern corner of the shelf (Weisberg and He, 2003). The intrusion of nutrients led to a domination of diatoms through the spring and summer months on the shelf (Walsh et al., 2003).

In early May, atmospheric iron supply was low (Fig. 9). Bottom concentrations combined with the initial boundary conditions (Tables 2 and 3) provided enough iron to supply a calculated *Trichodesmium* biomass in May of ~1.5 mg chl *a* m^{-2} along the outer shelf before depletion of both dFe and phosphorus (Fig. 8). Surface PO_4 distributions were <0.01 μmol PO_4 kg^{-1} at a distance of >20 km from the Florida coast (Lenes et al., 2001). The molar DIN/PO_4 ratios (Fig. 5) were >15 along the northern shelf, while ratios were <15 south of 28° latitude and along the shelf break. The simulated molar DIN/PO_4 ratios (Fig. 10) reproduce this pattern.

By June, surface concentrations ranged from 0.0 to 0.8 μmol PO_4 kg^{-1} across the WFS (Fig. 4a), with the maximum measured near shore. As much as 0.2 μmol PO_4 kg^{-1} was measured at the end of the Ft. Myers transect above the 50-m isobath. Surface PO_4 concentrations doubled inside the 50-m isobath (Fig. 4a). These phosphorus pools and a June influx of dust (Fig. 3) fueled the large *Trichodesmium* population increase measured in July (Fig. 6b).

The simulated surface and bottom DIN/PO_4 ratios of <15 on 7 June (not shown) indicated nitrogen limitation of diatoms to the 200-m isobath. The 7 June depth-integrated *Trichodesmium* chlorophyll biomass (Fig. 11a) had decreased by half from May (Fig. 8a). A similarly, measurements decreased from ~5 colonies l^{-1} in May (Fig. 6) to ~3 colonies l^{-1} in June during ECOHAB cruises. During June, increased atmospheric dust (Fig. 9) had led to increased surface dFe concentrations inside the 100-m isobath (Fig. 11b). Measured distributions of PO_4 and DOP showed phosphorus stripping as *Trichodesmium* biomass increased after Fe-fertilization between June and July (Fig. 4). In the model, PO_4 distributions >20 km from the West Florida coast rarely exceeded 0.1 μmol kg^{-1} (Fig. 11c). Thus, nutrient constraints of *Trichodesmium* growth along the WFS had switched from Fe- to P-limitation.

Lenes et al. (2001) reported a maximum *Trichodesmium* biomass of ~20 colonies l^{-1} over the 100-m isobath in July 1999 (Fig. 6b), a 100-fold increase from background concentrations of 0.1–0.2 colonies l^{-1} found in May 1999 (Fig. 6a). This maximum amounted to a pigment biomass of 0.7 μg chl *a* l^{-1}, representing ~50% of the observed chlorophyll stocks. A September maximum

Table 3
Open boundary conditions

Depth (m)	P_1 (mmol C m^{-3})	P_2 (mmol C m^{-3})	NH_4 (mmol m^{-3})	NO_3 (mmol m^{-3})	PO_4 (mmol m^{-3})	DON (mmol m^{-3})	DOP (mmol m^{-3})	DOC (mmol m^{-3})
1	0.125	0.02	0.1	0.05	0.05	6	0.05	55
10	0.125	0.02	0.1	0.05	0.05	6	0.05	55
50	0.125	0.01	0.1	0.05	0.05	6	0.05	55
100	0.125	0	0.1	0.05	0.05	6	0.05	55
150	0.125	0	0.1	0.05	0.05	6	0.05	54
200	0	0	0.1	5.04	0.24	6	0.05	53
250	0	0	0.1	7.55	0.375	6	0.05	52
300	0	0	0.1	9.06	0.5	6	0.05	51
350	0	0	0.1	10.57	0.595	6	0.05	50
400	0	0	0.1	12.08	0.68	6	0.05	49
450	0	0	0.1	13.59	0.765	6	0.05	48
500	0	0	0.1	15.1	0.85	6	0.05	47
600	0	0	0.1	18.12	1.02	6	0.05	46
700	0	0	0.1	21.14	1.19	6	0.05	45
800	0	0	0.1	24.16	1.36	6	0.05	45
900	0	0	0.1	27.18	1.53	6	0.05	45
1000	0	0	0.1	27.5	1.75	6	0.05	45
1500	0	0	0.1	30	1.75	6	0.05	45
2000	0	0	0.1	35	1.75	6	0.05	45
2500	0	0	0.1	40	1.75	6	0.05	45

Depth (m)	DIC (mmol m^{-3})	Z_1 (mmol C m^{-3})	B_1 (mmol C m^{-3})	B_2 (mmol C m^{-3})	D_1 (mmol C m^{-3})	D_2 (mmol C m^{-3})	dFe (mmol m^{-3})	cFe (mmol m^{-3})
1	2100	0	0.05	0.05	0.005	0.005	0.0003	0.0003
10	2100	0	0.05	0.05	0.005	0.005	0.0003	0.0003
50	2100	0	0.05	0.05	0.005	0.005	0.0003	0.0003
100	2100	0	0.05	0.05	0.005	0.005	0.0003	0.0003
150	2100	0	0.05	0.05	0.005	0.005	0.0004	0.0004
200	2120	0	0.05	0.05	0.005	0.005	0.0005	0.0005
250	2125	0	0.05	0.05	0.005	0.005	0.0005	0.0005
300	2130	0	0.05	0.05	0.005	0.005	0.0005	0.0005
350	2135	0	0.05	0.05	0.005	0.005	0.0006	0.0006
400	2140	0	0.05	0.05	0.005	0.005	0.0006	0.0006
450	2145	0	0.05	0.05	0.005	0.005	0.0006	0.0006
500	2150	0	0.05	0.05	0.005	0.005	0.0007	0.0007
600	2160	0	0.05	0.05	0.005	0.005	0.0007	0.0007
700	2170	0	0.05	0.05	0.005	0.005	0.0008	0.0008
800	2180	0	0.05	0.05	0.005	0.005	0.0008	0.0008
900	2190	0	0.05	0.05	0.005	0.005	0.0009	0.0009
1000	2200	0	0.05	0.05	0.005	0.005	0.0009	0.0009
1500	2200	0	0.05	0.05	0.005	0.005	0.001	0.001
2000	2200	0	0.05	0.05	0.005	0.005	0.001	0.001
2500	2200	0	0.05	0.05	0.005	0.005	0.001	0.001

Table 4
Nutrient and chlorophyll ratios for each functional group

Functional group	Carbon:Nitrogen	Carbon:Phosphorus	Carbon:Iron	Carbon:Chlorophyll
Diatoms (P_1)	6.625	106	7000	45
Trichodesmium (P_2)	6	144	1500	220
Bacteria (B)	6.625	200	15,000	–

of ~10 colonies l^{-1} measured above the 10-m isobath off Charlotte Harbor had disappeared by October (Lenes et al., 2001).

Walsh et al. (2006) assumed a mature colony size of $\sim 3 \times 10^4$ cells (Carpenter, 1983), a PC/chl *a* weight ratio of 220 (Carpenter, 1983), a PC/PN molar ratio of 6.1 (McCarthy and Carpenter, 1979), and a cellular chlorophyll content of 1.2×10^{-6} (Borstad, 1982) to calculate the potential particulate nutrient stocks (10.9 μmol PN kg^{-1} and 0.5 μmol PP kg^{-1}) associated with the observed decrement in population size. These values were consistent with nutrient concentrations measured within a decaying *Trichodesmium* bloom off St. Pete Beach, FL during May 2000 of 36.9 μmol DON kg^{-1}, 15.9 μmol NH_4 kg^{-1}, and 0.2 μmol PO_4 kg^{-1}.

By 6 July, the simulated DIN/PO_4 ratios (Fig. 12a) increased along the southern outer shelf. This coincided with the release of DON and ammonium during cellular respiration of the *Trichodesmium* population on the outer shelf into the 50-m isobath (Fig. 12b). The shelf-wide shift to higher DIN/PO_4 ratios continued between July and August (Fig. 13a). The simulated *Trichodesmium* biomass reached a 6-month maximum of ~10 mg chl *a* m^{-2} in August (Fig. 13b), a few weeks after the measured maximum (Fig. 6b). In contrast, a second model case with no atmospheric iron input reached a maximum *Trichodesmium* biomass in May after exhaustion of Fe stocks. DIN/PO_4 ratios (Fig. 13a) increased at sites distant from the coastal nutrient supplies and coincident with areas of high (>2 mg chl *a* m^{-2}) *Trichodesmium* biomass (Fig. 13b).

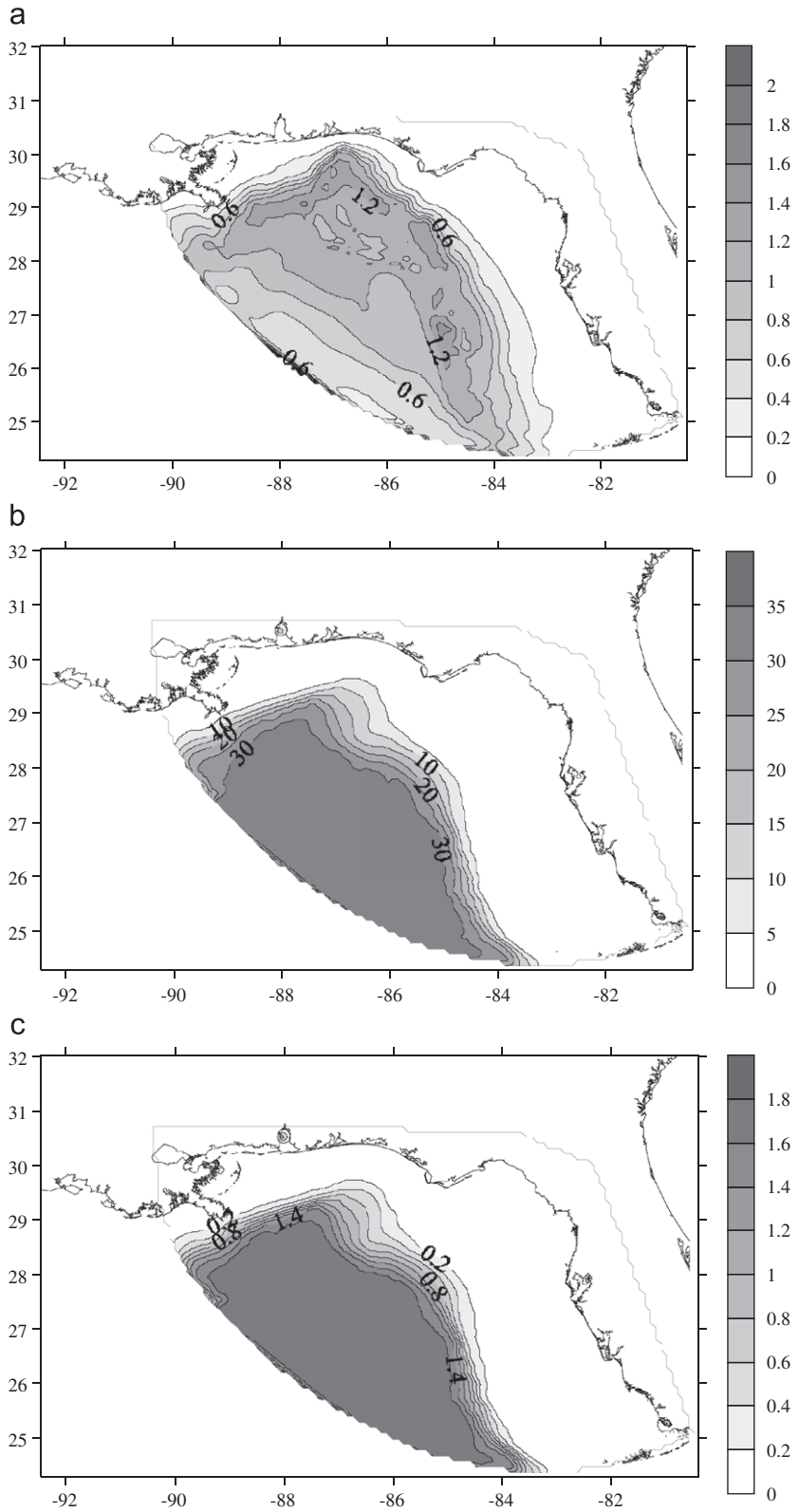

Fig. 8. The simulated (a) *Trichodesmium* depth-integrated chlorophyll biomass (mg chl $a\,m^{-2}$), (b) bottom nitrate+nitrite ($\mu mol\,NO_3\,kg^{-1}$), and (c) bottom phosphate ($\mu mol\,PO_4\,kg^{-1}$) on 4 May 1999.

Several low DIN/PO_4 areas were found in the absence of high cyanophyte biomass (Fig. 13a). Similarly, the measured DIN/PO_4 ratios had increased along the mid-shelf region by August (Fig. 5c).

Nitrogen fixation rates were as high as $\sim 700\,\mu mol\,N\,m^{-2}\,d^{-1}$ in August (not shown). Excretion/respiration and cell death supplied 'new' N to the water column in the form of DON and NH_4 which was converted to NO_3 by bacteria. A substantial build up

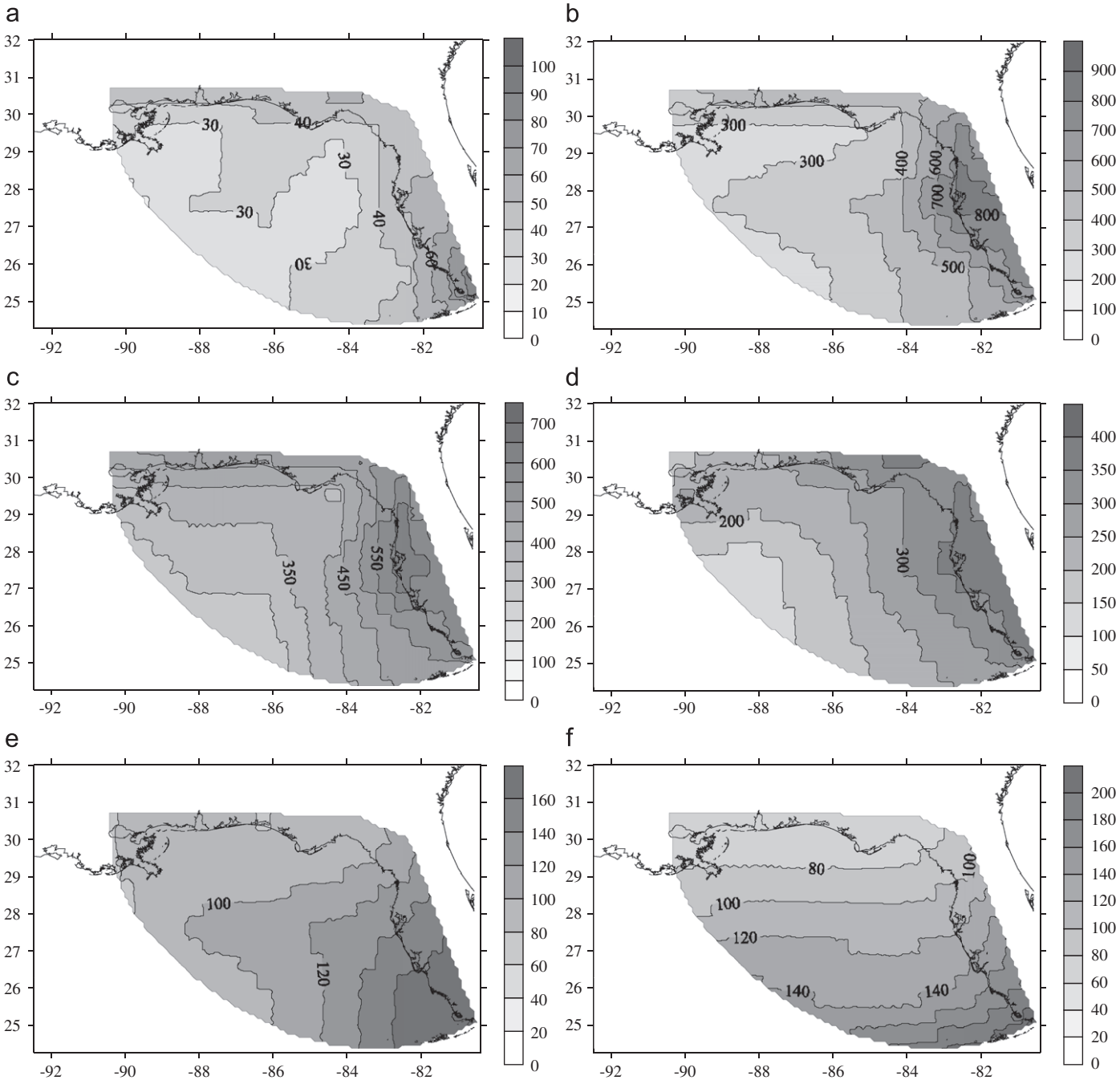

Fig. 9. Total monthly dust deposition as calculated by the model at each grid cell (mg dust m^{-2} $month^{-1}$) for the months of (a) May, (b) June, (c) July, (d) August, (e) September, and (f) October 1999 (after Lenes, 2006).

of NO_3 was not observed in the model due to the quick growth response of diatoms (Fig. 14a). August concentrations were $>1\,\mu mol\,NO_3\,kg^{-1}$ in the area of maximum *Trichodesmium* (Fig. 12b) and diatom (Fig. 14a) biomass. The northern shelf supported $>2\,\mu g\,chl\,a\,l^{-1}$ of diatoms in the outflow of the Mississippi River adjacent to the coast (Walsh et al., 2006). The 'new' N provided via atmospheric N_2 fixation increased the simulated offshore DIN/PO_4 ratios. Silica (Si) was not included as a state variable in the model, so diatoms were free to utilize this offshore bioavailable nitrogen source, doubling their surface biomass from $\sim 0.3\,\mu g\,chl\,a\,l^{-1}$ in July to $\sim 0.6\,\mu g\,chl\,a\,l^{-1}$ by August (Fig. 14a).

The model results showed that the highest surface chlorophyll ratio of *Trichodesmium* to diatoms (~0.8) was restricted to the edge of the southern WFS (Fig. 14b). The simulated dominance of >50% diazotrophs expanded shoreward as far as the 40-m isobath. This overlies the area of predicted *K. brevis* initialization (Walsh et al., 2006). Instead, diatoms dominated the shelf adjacent to the Mississippi River (Fig. 14a), with <30% diazotrophs at the northern shelf break despite depth-integrated *Trichodesmium* concentrations $>6\,mg\,chl\,a\,m^{-2}$ (Fig. 14b).

Mulholland and Capone (2000) reported C-based doubling times of ~2–14 d (specific growth rate: 0.05–0.32 d^{-1}) for cultures of *Trichodesmium* under a range of nutrient and light levels. Ambient stocks of $<0.1\,\mu mol\,PO_4\,kg^{-1}$ (Lenes et al., 2001) explained low, but consistent *in situ* growth rates ($<0.12\,d^{-1}$) measured during ECOHAB surveys along the mid- to outer shelf.

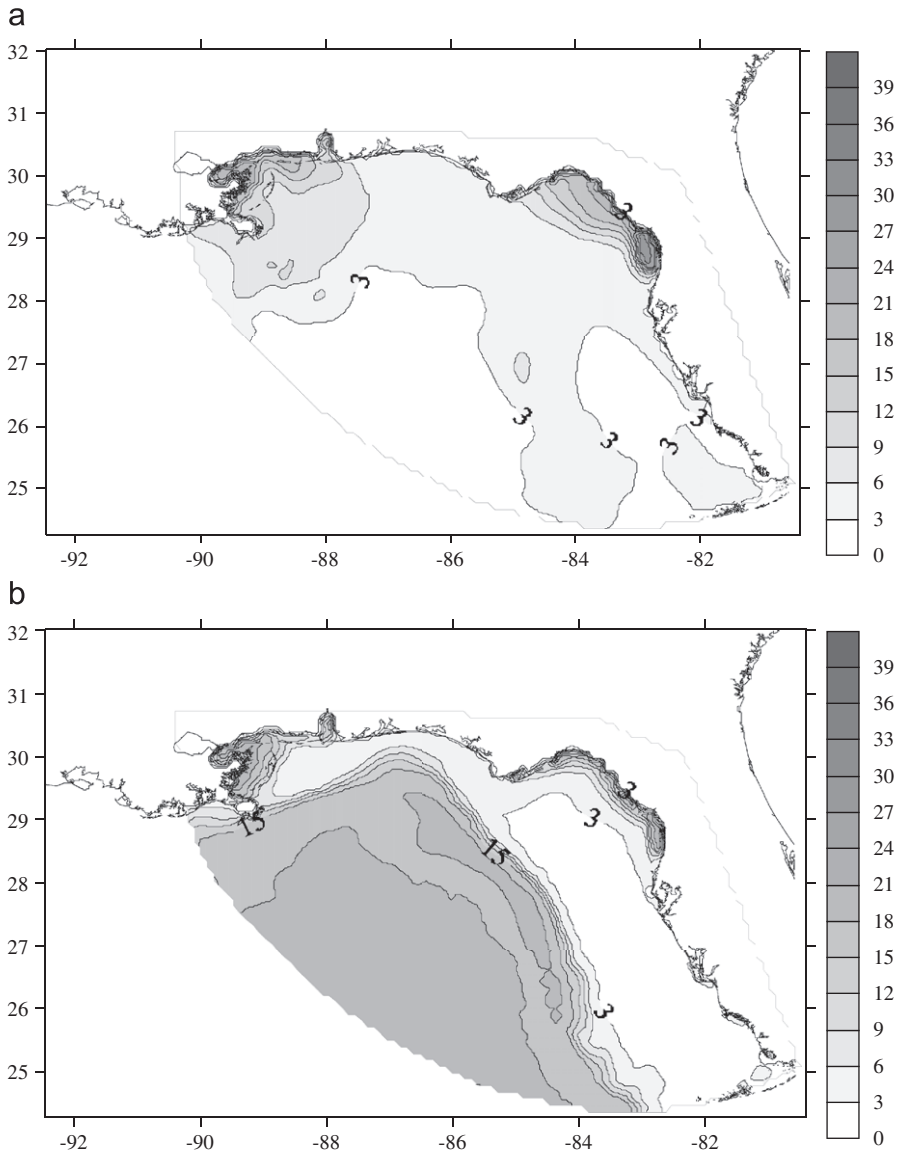

Fig. 10. The simulated molar DIN/PO_4 ratios (mol/mol) calculated at the (a) surface and (b) bottom on 4 May 1999.

These were similar to growth rates of *Trichodesmium* populations measured in the oligotrophic subtropical/tropical Atlantic (Carpenter, 1983). Based on a PO_4 half-saturation constant of 0.1 μmol PO_4 kg^{-1} (Walsh and Steidinger, 2001), a 40% respiration/excretion rate (Lenes et al., 2005), and a maximum growth rate of 0.7 d^{-1} (Walsh and Steidinger, 2001), a *Trichodesmium* population would need constant access to ~0.04 μmol P kg^{-1} to maintain a realized growth rate of 0.12 d^{-1}. In areas of higher P concentrations, the model predicted growth rates up to ~0.3 d^{-1}.

A further increment in DIN/PO_4 ratios had occurred by September as the simulated *Trichodesmium* population decreased as nutrient supply decreased (Fig. 15). A decrease in atmospheric Fe (Fig. 9) led to release of particulate N and P stocks to the water column. Depth-integrated *Trichodesmium* biomass was reduced to <2.7 μg chl *a* l^{-1} by September (Fig. 15b), a 73% decline. A transition to southwesterly winds in the fall forced cross-shelf bottom Ekman transport toward the coast in coastal upwelling (Weisberg and He, 2003). Therefore, the ~7.3 μg chl *a* l^{-1} reduction in *Trichodesmium* biomass represented a particulate nutrient pool of ~22.3 μmol N kg^{-1} and ~0.9 μmol P kg^{-1} (Table 5). Loss of the final ~2.7 μg chl *a* l^{-1} between September and October provided another ~8.3 μmol N kg^{-1} and ~0.3 μmol P kg^{-1}.

Walsh et al. (2006) predicted the initiation of *K. brevis* blooms on the WFS was near bottom along the 30-m isobath between Tampa Bay and Naples, within ~40 km from the major fluvial sources of phosphorus. In October 1999, ~20 μg chl *a* l^{-1} of *K. brevis* was measured within near-shore waters above the 10-m isobath between Tampa Bay and Charlotte Harbor. This would require access to a minimum dissolved nitrogen and phosphorus supply of ~12.5 μmol N kg^{-1} and ~0.6 μmol P kg^{-1} (Table 5). Therefore, 41% and 50% of the simulated *Trichodesmium*-derived nitrogen and phosphorus could support the observed *K. brevis* biomass.

3.2. Water column iron

The model's surface total dissolved iron (dFe) concentrations matched the general observed pattern from data collected during monthly ECOHAB cruises in 1999 (Fig. 2). Both the measured (Fig. 2)

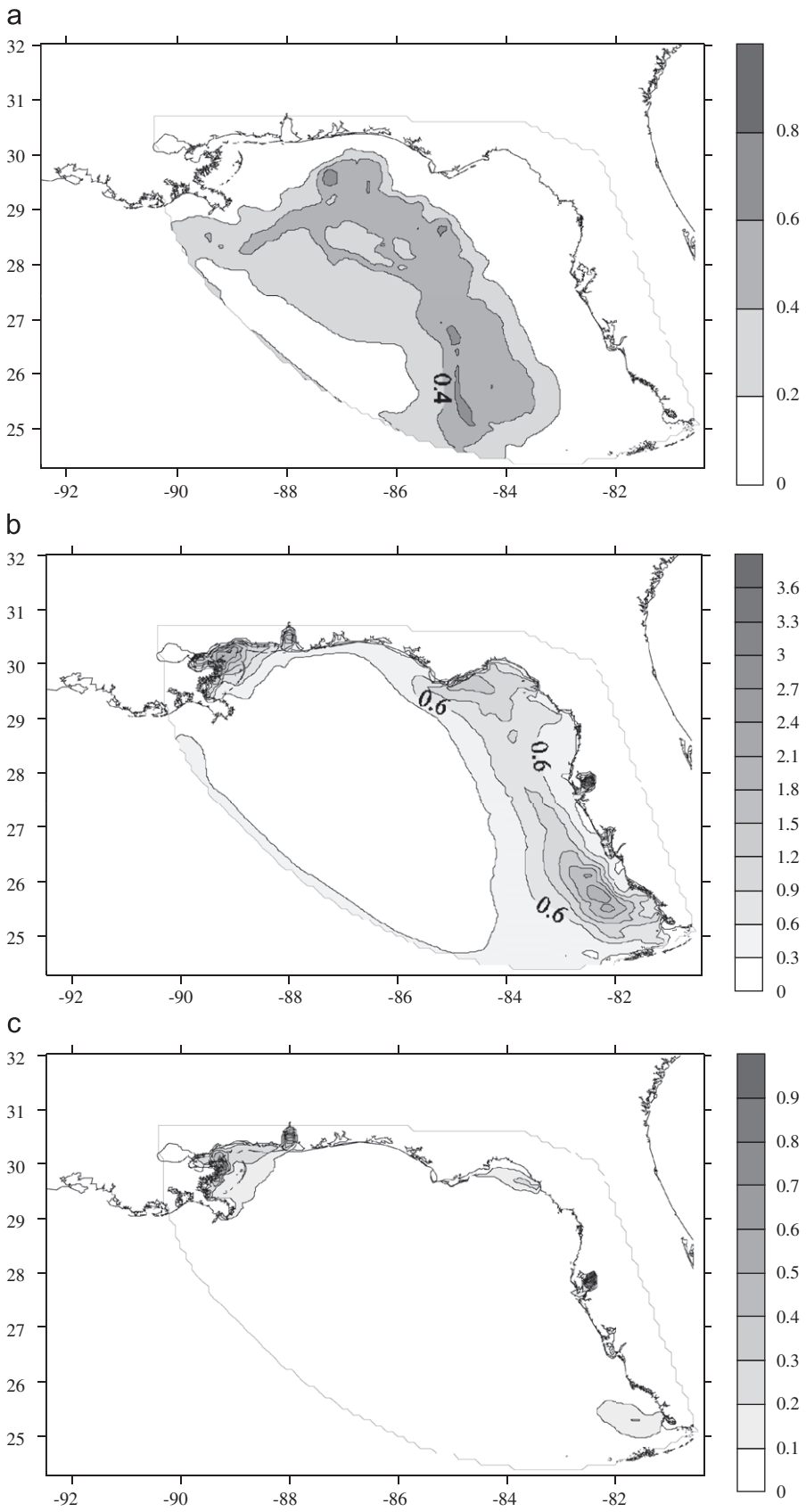

Fig. 11. The simulated (a) *Trichodesmium* depth-integrated chlorophyll biomass (mg chl *a* m^{-2}), (b) total dissolved iron (dFe) in the surface sigma layer (nmol Fe kg^{-1}), and (c) surface distributions of phosphate (μmol PO_4 kg^{-1}) on 7 June 1999.

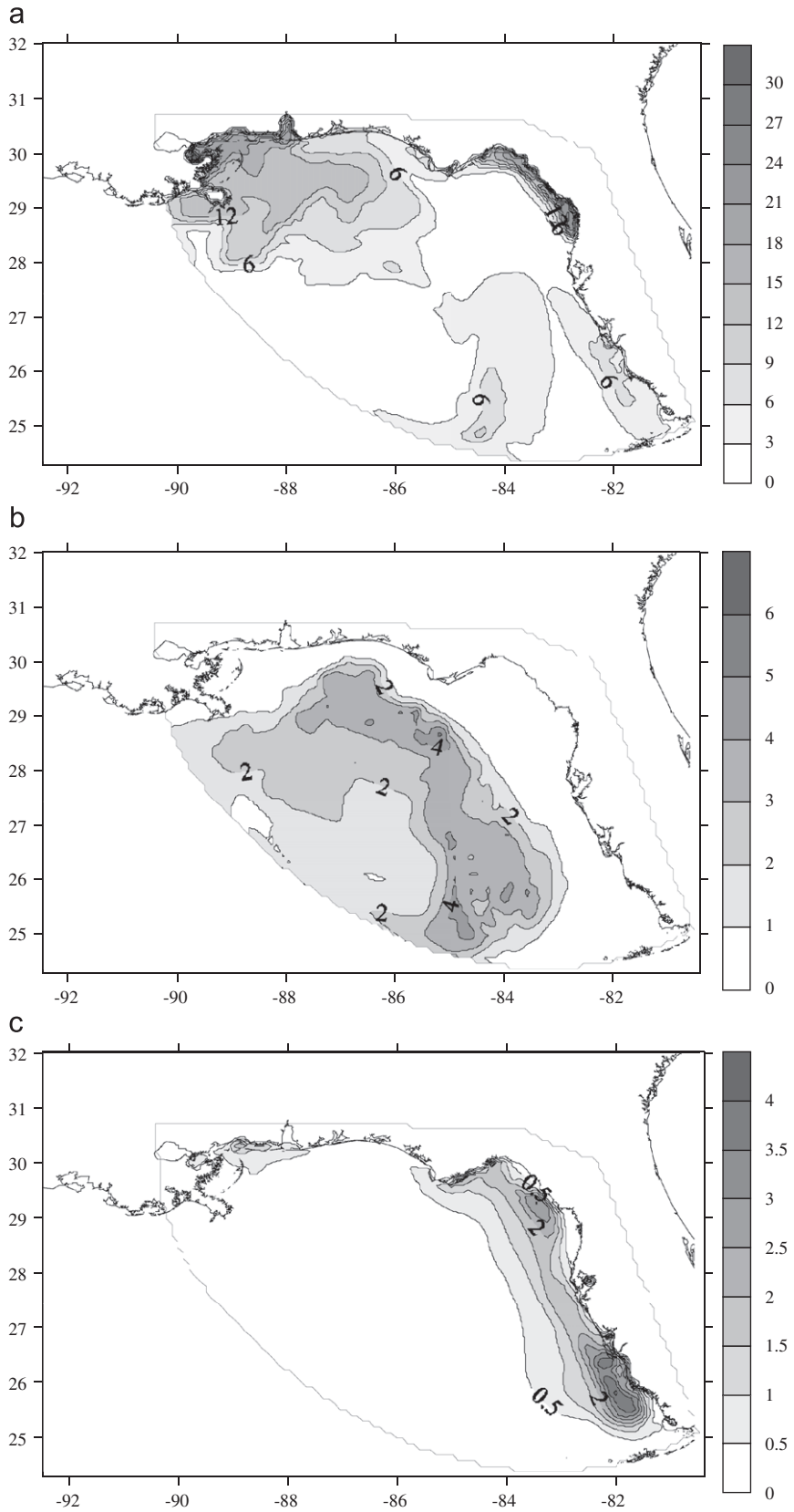

Fig. 12. The simulated (a) surface DIN/PO_4 molar ratios (mol/mol), (b) depth-integrated *Trichodesmium* chlorophyll biomass (mg chl *a* m^{-2}) and (c) total dissolved iron (dFe) in the surface sigma layer (nmol Fe kg^{-1}) on 6 July 1999.

and simulated dFe concentrations were <0.5 nmol kg^{-1} during early May 1999 over most of the WFS. The simulated dFe concentrations were >1 nmol Fe kg^{-1} near the mouth of the Mississippi River, along the Big Bend region, and near Naples. By 7 June, the measured (Fig. 2b) and simulated (Fig. 12b) coastal dFe stocks near Naples had drifted north and farther offshore (~20–30 km).

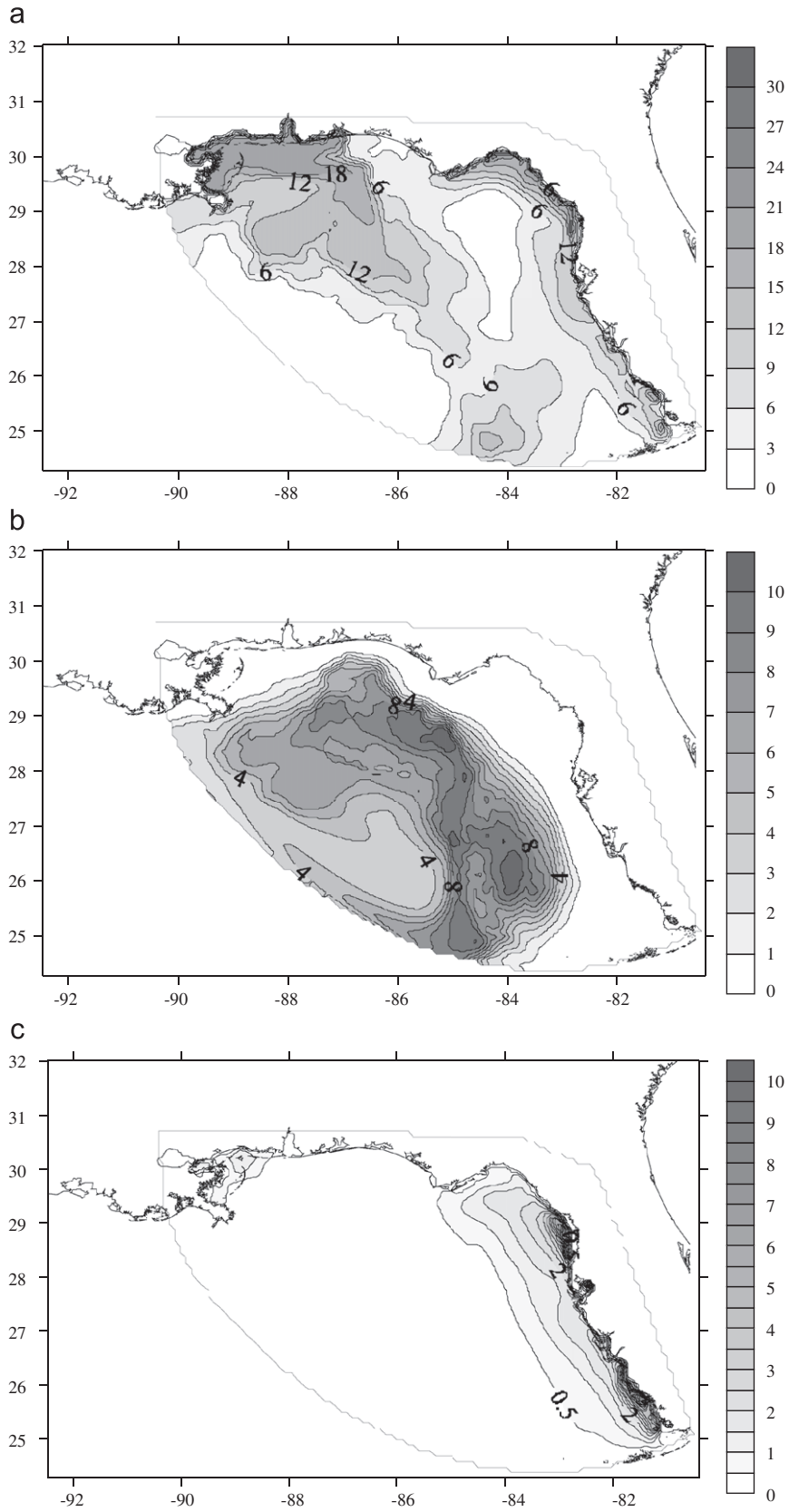

Fig. 13. The simulated (a) surface DIN/PO_4 molar ratios (mol/mol), (b) depth-integrated *Trichodesmium* chlorophyll biomass (mg chl *a* m^{-2}) and (c) total dissolved iron (dFe) in the surface sigma layer (nmol Fe kg^{-1}) on 7 August 1999.

The wet deposition event on 25–27 June 1999 provided 125–476 nmol particulate Fe kg^{-1} (Lenes, 2006) over the model domain with the highest input along the Florida coast (Fig. 9). Therefore, 6.3–23.8 nmol Fe kg^{-1} was added to the surface dFe pool (5% iron dissolution). Ten days later on 5–7 July 1999, dFe concentrations of >2 nmol kg^{-1} were measured during ECOHAB:

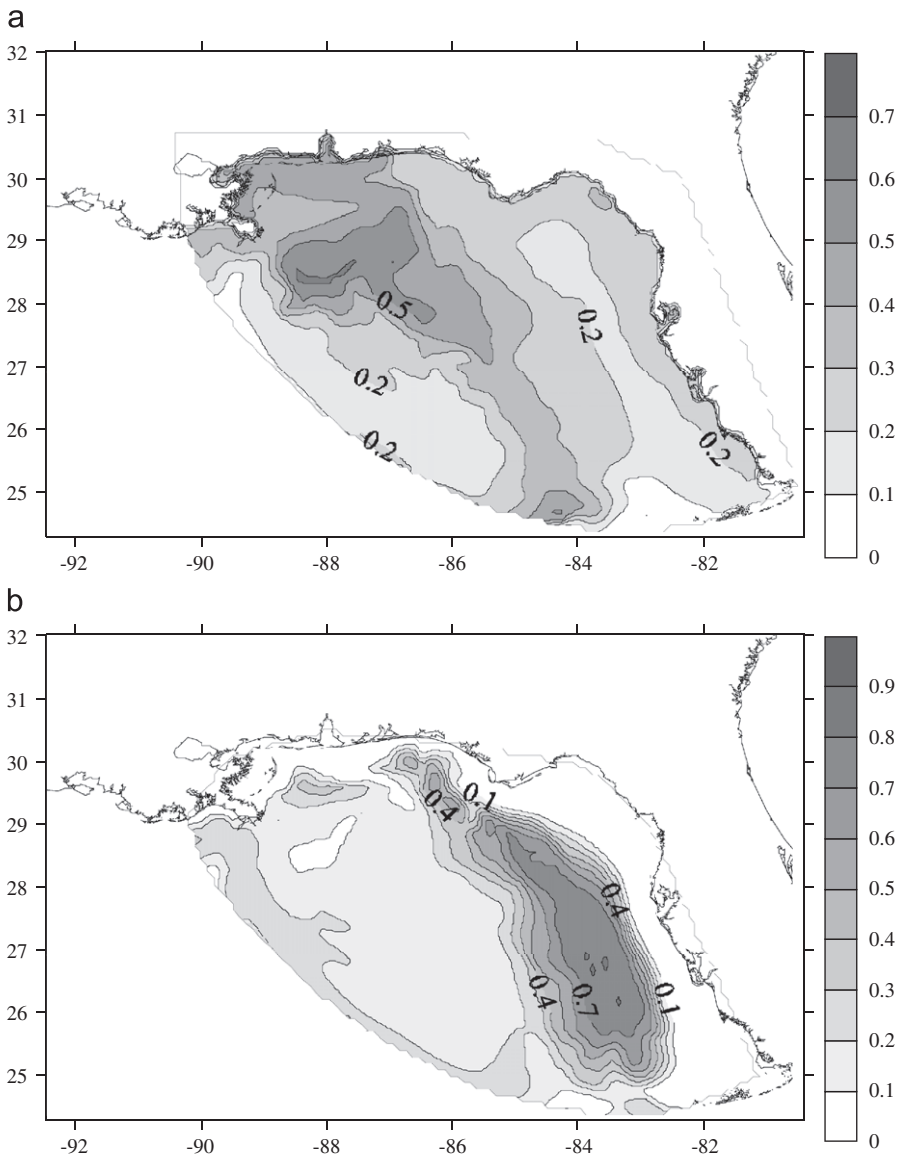

Fig. 14. The simulated (a) surface diatom chlorophyll biomass (μg chl $a\,l^{-1}$) and (b) the *Trichodesmium*/diatom surface chlorophyll ratio (chl *a*/chl *a*) on 8 August 1999.

Florida shoreward of the 50-m isobath, with the highest coastal dFe concentrations of ~4 nmol Fe kg^{-1} along the 20-m isobath offshore of Charlotte Harbor (Fig. 2c). The simulation produced dFe concentrations of ~4 nmol Fe kg^{-1} by 6 July 1999 SSE of Charlotte Harbor between the 20- and 30-m isobaths (Fig. 13c).

The simulated dFe concentrations had decreased by as much as 40% from July to August as monthly deposition began to diminish (Fig. 9). The measured (Fig 2d) and simulated (Fig. 13c) dFe values were still >2 nmol Fe kg^{-1} shoreward of the 50-m isobath. By 7–9 September, both measured (Fig. 2e) and simulated (Fig. 15c) dFe concentrations had dropped to <1.5 nmol kg^{-1} shoreward of the 50-m isobath, while the dFe pool had returned to background (<0.5 nmol kg^{-1}) by 5–7 October (Fig. 2f).

We ran a null case of the model to test the impact of riverine versus atmospheric dust input. In the null case, there was no atmospheric deposition of iron so that only the deep-sea, riverine, and bottom boundaries supplied iron to the biochemical model. Since the contribution of both the deep-sea component and bottom boundary were minimal due to strong summer stratification, the surface Fe concentration was driven mainly by fluvial inputs.

These results indicated that both atmospheric deposition and riverine supplies were important sources of iron to the WFS. In the summer and fall of 1999, the fluvial dFe stocks drifted along the coast (not shown) in response to the seasonal change in wind direction (Weisberg and He, 2003). Since dFe concentrations in the null case were below background over most of the model domain, the primary producers were consistently Fe-limited. Therefore, the dFe concentrations and *Trichodesmium* biomass of the full simulation (atmospheric deposition and river boundaries) most closely matched the data collected during the 1999 monthly ECOHAB cruises (Figs. 2, 6).

4. Conclusions

The transport of Saharan dust across the N. Atlantic delivered iron to the Gulf of Mexico (Fig. 3). Enrichment of surface waters above the WFS increased the availability of iron for the marine diazotroph, *Trichodesmium* spp. Consequently, the growth rate became a function of P acquisition. Late spring and early summer

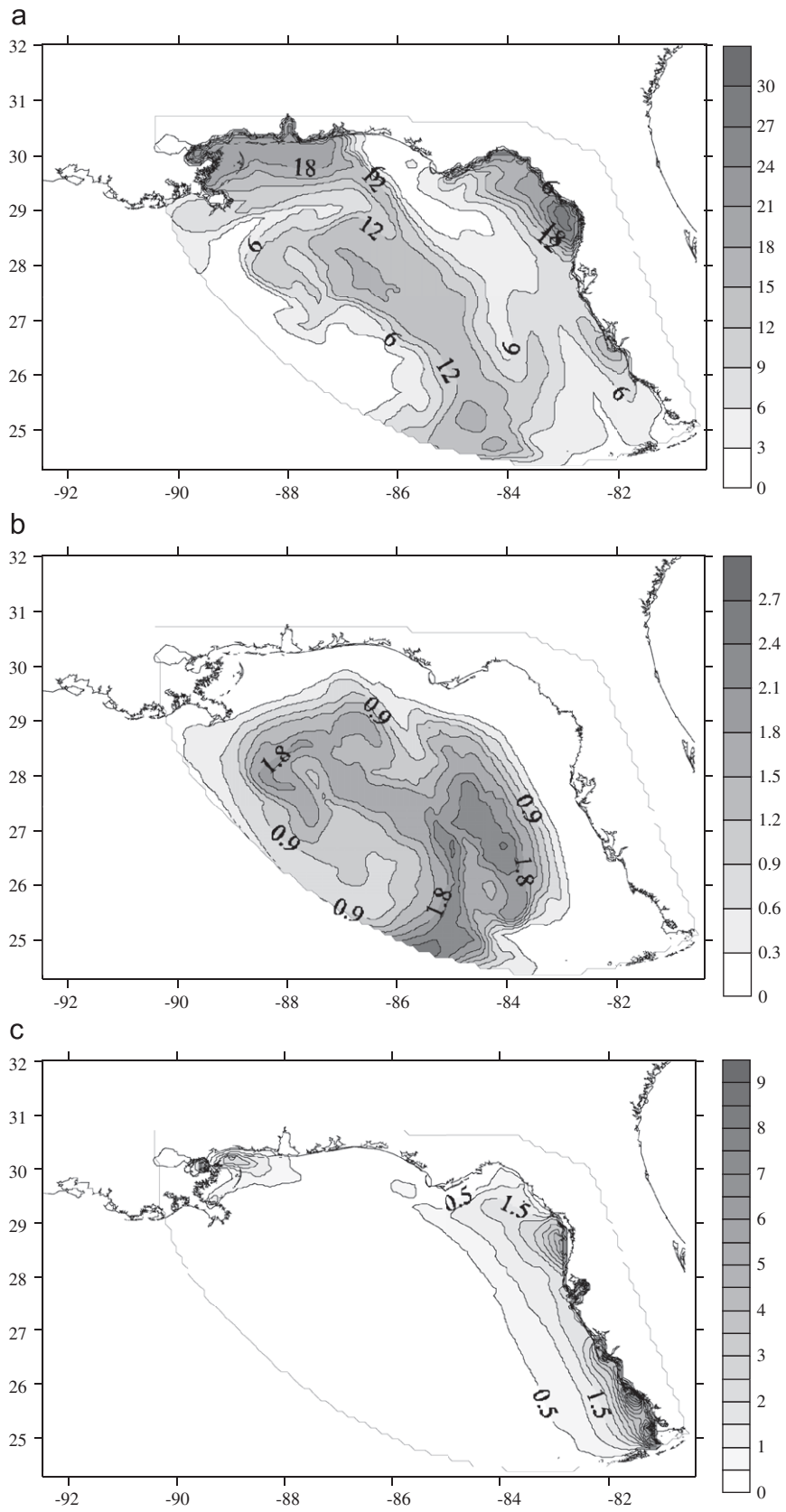

Fig. 15. The simulated (a) surface DIN/PO_4 molar ratios (mol/mol), (b) depth-integrated *Trichodesmium* chlorophyll biomass (mg chl *a* m^{-2}) and (c) total dissolved iron (dFe) in the surface sigma layer (nmol Fe kg^{-1}) on 8 September 1999.

Table 5
The potential nutrient transfer supplied by the simulated fall reduction in *Trichodesmium* biomass at the 30-m isobath off Charlotte Harbor to the observed *Karenia brevis* population

August-to-September	September-to-October	Total particulate loss	Observed *K. brevis*
−7.3 mg chl *a* m^{-2}	−2.7 mg chl *a* m^{-2}	10 mg chl *a* m^{-2}	20 ug chl *a* l^{-1}
+22.3 mmol N m^{-2}	+8.3 mmol N m^{-2}	30.6 mmol N m^{-2}	12.5 μmol N kg^{-1}
+0.9 mmol P m^{-2}	+0.3 mmol P m^{-2}	1.2 mmol P m^{-2}	0.6 μmol P kg^{-1}

P concentrations on the oligotrophic WFS were $<0.1\,\mu mol\,kg^{-1}$, except near the coast where river P sources maintained elevated P stocks of $>0.2\,\mu mol\,kg^{-1}$ inside the 10-m isobath (Fig. 4). In the model, the WFS water column had molar N:P ratios <6 in late spring (Fig. 10).

According to the model, nitrogen fixation gave *Trichodesmium* a competitive advantage over other phytoplankton species (Fig. 14). Upon removal of Fe-limitation, a near-shore *Trichodesmium* population should increase from fluvial P supplies since phosphorus availability controlled growth rates and maximum biomass. The model did not reproduce this pattern due to competition along the coast with faster growing diatoms even though a small *in situ* increment occurred during July 1999. Instead, the model's *Trichodesmium* population slowly increased over the shelf break during June (Fig. 11a) and July 1999 (Fig. 12a), in response to uptake of ambient P stocks (Fig. 11c). The model successfully simulated the seasonal peak of depth-integrated biomass in August (~10 mg chl *a* m^{-2}) between the 50- and 100-m isobaths (Fig. 13a).

Trichodesmium, because of its (modeled) vertical migration, had access to the total integrated water column P stocks. Initially, *Trichodesmium* made use of offshore phosphorus. Then, as advective transport carried a portion of the population toward the coast between Tampa Bay and Charlotte Harbor at the end of the summer, the diazotrophs used fluvial P stocks. Nitrogen fixation rates vary as a function of internal P more than internal Fe (Sanudo-Wilhelmy et al., 2001). Therefore, P-availability controlled both maximum biomass and net nitrogen fixation rates.

The simulated decrease in *Trichodesmium* biomass of ~7.3 mg chl *a* m^{-3} (Figs. 13b, 15b) as Fe-fertilization decreased during the fall transition (Fig. 9) provided adequate particulate nutrient stocks to initialize the ~20 μg chl *a* l^{-1} of *K. brevis* measured between Tampa Bay and Charlotte Harbor in October (Table 5). During the simulation, surface molar N:P ratios in this area had increased to near Redfield (Fig. 15a). Therefore, the WFS combined low molar N:P river systems and far-field aeolian dust to create an ecosystem capable of supplying enough 'new' nitrogen via N_2 fixation to initialize blooms of *K. brevis*. Additionally, the physiological dynamics of *Trichodesmium* had simulated biomass increments (Fig. 13) and nitrogen fixation rates far greater than predicted from surrounding nutrient stocks.

Therefore, temporal variability in dust supply and precipitation play a crucial role for Fe on the WFS. Both short term (year-to-year) and long-term changes linked to climate can modulate regional dust deposition (Prospero and Lamb, 2003). The variability in Fe delivery would have a significant impact on *Trichodesmium* biomass, and subsequently, *K. brevis*. Further studies are needed to better quantify both dust deposition and water column Fe dynamics.

Acknowledgments

This analysis is Center for Prediction of Red Tides (CPR) interagency contribution # 1 funded by Grants R-ESSF/03-0000-0039 to JML from the National Aeronautics and Space Administration as part of the Earth Systems Science Fellowship program, NNG04GL55G to KLC and NNG04GG04G to FMK from the National Aeronautics and Space Administration, OCE 0095970 to CAH from the National Science Foundation as part of the DOTGOM program, N00014-96-1-5024 to KAF and JJW, and N00014-98-1-0158 to RHW from the Office of Naval Research as part of the HyCODE and FSLE programs, 1435-01-97-CT-30851 to AEJ from the Minerals Management Service for the NEGOM program, as well as State of Florida funds to FWRI and USF. I would also like to thank the Tropical Rainfall Measurement Mission and National Center of Environmental Prediction for precipitation data.

Appendix A. Optics

Spectral irradiance at depth, $I_{z(\lambda)}$, was calculated according to Beer's law of exponential decay:

$$I_{z(\lambda)} = I_{0(\lambda)} e^{-k_\lambda z} \tag{4}$$

where λ represented a specific wavelength. k_λ was the attenuation coefficient for that wavelength defined as

$$k_\lambda = \frac{k_{w(\lambda)} + \sum\left(k_{A(\lambda)} \int_0^z A(z)\mathrm{d}z\right)}{z} \tag{4a}$$

where A denoted each optically significant functional group, i.e. diatoms (P_1), cyanophytes (P_2), bacteria ($B = B_1{+}B_2$), detritus ($D = D_1{+}D_2$), and CDOM. Their specific attenuation coefficients ($k_{A(\lambda)}$) were represented by $k_{P1(\lambda)}$, $k_{P2(\lambda)}$, $k_{B(\lambda)}$, and $k_{C(\lambda)}$; while $k_{w(\lambda)}$ was the total attenuation coefficient for water (Smith and Baker, 1981; Pope and Fry, 1997).

Attenuation coefficients for phytoplankton (Subramaniam et al., 1999), bacteria (Morel and Ahn, 1990), and detritus (Roesler et al., 1989) were equal to the sum of the wavelength-specific absorption coefficients and the associated scattering coefficients. As for CDOM, backscattering was ignored due to its dissolved nature and generally high absorption values (Gordon et al., 1988). The CDOM attenuation coefficients were equal to published CDOM absorption coefficients in the eastern Gulf of Mexico (Carder et al., 1989).

Appendix B. Biochemistry

B.1. Biology

B.1.1. Primary producers

The dynamics of a general pelagic diatom pool (P_1) and the cyanobacterium *Trichodesmium* spp. (P_2) were modeled, with the rate of change in biomass (mmol C m^{-3}) over time (t) described by

$$\frac{\partial P_n}{\partial t} = Tr_t(\mathrm{d}P_n) - \frac{\partial}{\partial \sigma}(w_n P_n) + \mathrm{d}(\mu_n P_n - \varepsilon_n P_n - \psi_n P_n - \gamma_n r_n P_n - \chi_n P_n) \tag{5}$$

where w_1 was the sinking rate of pelagic diatoms and w_2, the vertical migration rate of *Trichodesmium*. The terms μ_n, ε_n, ψ_n, γ_n, and χ_n represented the respective growth, respiration, excretion, grazing, and lysis rates. Sloppy grazing for both phytoplankton populations was accounted for via an ingestion term ($r_{3,4}$).

The realized net growth rate for *Trichodesmium*, μ_2, was determined by the least available resource of light or nutrients:

$$\mu_2 = \mu^T_{\max 2} \times \min \begin{bmatrix} (I_z/I_{sat} e^{(1-I_z/I_{sat})}), \\ (PO_4/\{k_{PO_4(n)} + PO_4\}) \\ +(DOP/\{k_{DOP(n)} + DOP\}), \quad \text{or} \\ (dFe/k_{dFe(n)} + dFe) \end{bmatrix} \tag{6}$$

where $\mu^T_{\max 2}$ was the maximum gross growth rate adjusted for temperature-stress, as *Trichodesmium* growth rate was maximum at temperatures $>20\,^{\circ}C$ (Carpenter, 1983). The Michaelis–Menten half-saturation constants for uptake of phosphate (k_{PO_4}), dissolved organic phosphorus (k_{DOP}), and iron (k_{dFe}) were specific to *Trichodesmium*. Phosphorus availability was calculated as total dissolved phosphorus (TDP = DOP+PO_4), where preferential uptake was given to phosphate over DOP through use of a smaller half-saturation constant (Table 1). High levels of alkaline phosphatase activity have been measured in association with phosphate-depleted colonies (Yentsch et al., 1972; Stihl et al., 2001), indicating *Trichodesmium* can assimilate DOP. I_{sat} was the saturation light intensity for *Trichodesmium*. Photo-inhibition was ignored due to high saturation light intensities (Carpenter and Roenneberg, 1995) and the ability to control their buoyancy in relation to the light field (Walsby, 1978; Villareal and Carpenter, 1990). Subramaniam et al. (1999) also showed that *Trichodesmium* releases excess energy as fluorescence and possesses high levels of photoprotective pigments.

The realized net growth rate of pelagic diatoms, μ_1, was determined by the same method, though nitrogen species were included

$$\mu_1 = \mu^T_{\max 1} \times \min \begin{bmatrix} (I_z/I_{sat} e^{(1-I_z/I_{sat})}), \\ (NO_3/\{k_{NO_3(n)} + NO_3\}), \\ (NH_4/\{k_{NH_4(n)} + NH_4\}), \\ (PO_4/\{k_{PO_4(n)} + PO_4\}), \quad \text{or} \\ (dFe/k_{dFe(n)} + dFe) \end{bmatrix} \tag{7}$$

where each half-saturation constant was specific to diatoms (Walsh et al., 2003). Diatoms were selected as a second phytoplankton species to compete with *Trichodesmium* for nutrient supplies. The biochemical model was formulated to investigate the pathways for growth and decay of a *Trichodesmium* population, and the subsequent effect on water column nutrient ratios.

The maximum phytoplankton gross growth rate varies with changes in temperature (Eppley, 1972):

$$\mu^T_{\max(n)} = \mu_{\max(n)} \exp^{0.0633(T-27)} \tag{8}$$

where T was the temperature obtained from POM and $\mu_{\max(n)}$ was the functional group-specific maximum growth rate (Table 1).

B.1.2. Loss terms

Grazing rates are low on populations of *Trichodesmium*, since only a few species of copepods can deal with the toxins (O'Neil and Roman, 1992; Sellner, 1997). Thus, *Trichodesmium* grazing (γ_2) was calculated as a linear function of biomass (Hood et al., 2001), removing 1% of the population per day. Diatom grazing (γ_1) was calculated as a Michaelis–Menten function after Mullin et al. (1975):

$$\gamma_1 = \gamma_1^{\max}((P_1 - P_1^{ref})/k_{zoo} + (P_1 - P_1^{ref})) \tag{9}$$

where $\gamma_1^{\max}$ was the maximum grazing rate and k_{zoo}, the half-saturation constant. P_1^{ref} represented the background reference population for *Trichodesmium* (0.01 mmol C m^{-3}) and diatoms (0.5 mmol C m^{-3}), below which grazing was set to zero.

Viruses can be a significant mode of mortality for single-cell marine cyanobacteria (Proctor and Fuhrman, 1990, 1991) and *Trichodesmium* spp. 0.3–6.5% of trichomes per day (Hewson et al., 2004). Berman-Frank et al. (2004) measured programmed cell death in *Trichodesmium* at a rate of >45% in 24 h with increased rates under nutrient, light, or oxidative stress. An exponential non-grazing mortality term (χ^2) was formulated as a negative function of phytoplankton limitation (Lenes, 2002):

$$\chi = 0.15 \exp^{-13.54 v_2} \tag{10}$$

where v_2 was the fraction of maximum uptake by *Trichodesmium* of Fe and P. Thus, as limitation of *Trichodesmium* growth becomes larger, their non-grazing mortality increases exponentially, reflecting other losses. These lysed materials are returned to the water column mainly as DOC, DON, and DOP, as well as dFe.

B.1.3. Vertical migration

Trichodesmium has been shown to vertically migrate throughout the euphotic zone in response to light levels, with significant populations observed at depths >100 m oligotrophic, clear waters (Borstad, 1982). As significant light becomes available, ballast is added through photosynthesis, causing the organism to sink. When light is no longer available, the ballast is respired, allowing the organism to float back to the surface. Previous simulations (Kromkamp and Walsby, 1992) suggest that trichomes and colonies may sink to these depths. Walsby (1992) indicated that sinking and floating velocities are often in excess 1 mm s^{-1}, depending upon colony size and form resistance. In this model, a constant migration rate of 0.9 mm s^{-1} operated as an on/off switch. The population sank when $I_z > 25\,\mu E\,m^{-2}\,s^{-1}$ and floated when $I_z < 25\,\mu E\,m^{-2}\,s^{-1}$. This underestimated the delay observed in migrating populations at the surface, but corrected for continued sinking below the light compensation depth. Diatoms had a constant sinking rate (Table 1).

B.1.4. Microbial loop

A large community of heterotrophic bacteria was often associated with populations of *Trichodesmium* (Carpenter and Price, 1977; Borstad, 1978; Capone et al., 1994). Sheridan et al. (2002) found bacterial enrichment of *Trichodesmium* colonies 2–5 times that of the water column. Increases in bacterial biomass were also found for unhealthy versus healthy colonies, verifying bacterial dependence on *Trichodesmium*'s dissolved organic exudates as a growth media (Sellner, 1997). Therefore, heterotrophic bacteria of the model both remineralize organic matter to inorganic matter, and nitrify ammonium to nitrate.

The bacterial population was broken into two functional groups: the ammonifying (B_1) and nitrifying (B_2) bacteria. These were described by

$$\frac{\partial dB_n}{\partial t} = Tr_t(dB_n) + d(\mu_n B_n - \varepsilon_n B_n - m_n B_n) \tag{11}$$

where $\varepsilon_{3,4}$ represented the bacterial respiration rates (del Giorgio and Cole, 2000) and m_n, the bacterial mortality rates (Table 1). The realized bacterial growth rates ($\mu_{3,4}$) were calculated as a Michaelis–Menten function of the least available nutrient, where ammonifying bacteria were limited by organic nutrients (DOC, DON, DOP) and nitrifying bacteria by inorganic nutrients (NH_4, PO_4).

B.2. Chemistry

B.2.1. Carbon

Peng et al. (1987) described the net CO_2 flux across the air–sea interface by

$$F(CO_2) = E(CO_2)\frac{\Delta pCO_2}{(pCO_2)_{air}} \quad (12)$$

where $E(CO_2)$ is the CO_2 gas exchange coefficient and ΔpCO_2, the difference between pCO_2 in seawater and air.

Utilization and remineralization of dissolved inorganic carbon (DIC) was then described as

$$\frac{\partial DIC}{\partial t} = Tr_t(dDIC) + d(-\upsilon_n P_n - \upsilon_2 B_2 + \varepsilon_n P_n + \varepsilon_n B_n + r_n \gamma P_n + k_{photo} DOC) \quad (13)$$

where DIC was a carbon source for *Trichodesmium*, diatoms, and the nitrifying bacteria, but not the ammonifying bacteria. DIC was respired by *Trichodesmium*, diatoms, and bacteria, and since grazers are not explicitly modeled, a small portion of grazed diazotrophs (r_1) and diatoms (r_2) were converted to DIC to compensate for grazer respiration. Photoconversion of dissolved organic carbon was the final source of DIC. At the surface boundary ($h = 0$), CO_2 flux is calculated from Eq. (17).

Dissolved organic carbon (DOC) was described as

$$\frac{\partial DOC}{\partial t} = Tr_t(dDOC) + d(-\upsilon_1 B_1 + m_n B_n + \psi_n P_n + (1 - r_{3,4})\gamma_n P_n + \chi_n P_n + k_d d_n + k_{fp} z_1 - bDOC) \quad (14)$$

where DOC was a carbon source for ammonifying bacteria. A fraction of grazed phytoplankton-bound carbon was released as DOC, representing sloppy grazing.

B.2.2. Nitrogen

As the underlying focus of this model, the nitrogen dynamics were critical in determining whether, under various scenarios, the WFS can produce a diazotrophic population large enough to support the observed red tide blooms of $>10\,\mu g\,chl\ a\,l^{-1}$ and $\sim 2\,g\,C\,m^{-2}\,d^{-1}$ (Vargo et al., 1987). Typical measurements of nitrogen fixation in the western Atlantic of $\sim 200\,mmol\,N\,m^{-2}\,yr^{-1}$ (Carpenter and Roman, 1991), or $\sim 0.5\,mmol\,N\,m^{-2}\,d^{-1}$, suggests a potential production by *Trichodesmium* of only $0.4\,g\,C\,m^{-2}\,d^{-1}$. Recent studies have shown western Atlantic nitrogen fixation is actually 4–5 times greater than previously thought (Capone et al., 2005; Lenes et al., 2005). This raises "new" production estimates to $1.6–2.0\,g\,C\,m^{-2}\,d^{-1}$, similar to those measured for red tide blooms in the Gulf of Mexico. Yet, *Trichodesmium* accumulations of $>100\,\mu g\,chl\ a\,l^{-1}$ have been found in the WFS (Walsh et al., 2003), suggesting either much higher rates of new production or mass accumulation along fronts or beaches.

Mulholland et al. (2001) demonstrated that *Trichodesmium* could assimilate inorganic nutrients (ammonium [NH_4^+] and nitrate [NO_3^-]) and amino acids (glutamate and glutamine) without significant suppression of nitrogen fixation. They suggest that this may be a possible mechanism for cell clusters containing nitrogenase (diazocysts) to provide N to non-nitrogen fixing regions of the trichomes. For purposes of this model, all required N would be supplied via N_2 fixation (function of primary production). Since *Trichodesmium* releases up to 50% of fixed nitrogen as DON (Glibert and Bronk, 1994), much of which in the form of amino acids (Capone et al., 1994), 25% of fixed-N was released as DON via excretion. The DON state equation mirrors that of DOC, with differences found only in the variation of N:C ratios (Table). Therefore, the state equation for ammonium was

$$\frac{\partial NH_4}{\partial t} = Tr_t(dNH_4) + d\frac{N}{C}(-\upsilon_1 P_1 - \upsilon_4 B_4 + \varepsilon_n P_n + \varepsilon_3 B_3 + r_{3,4}\gamma_n P_n + bDON) \quad (15)$$

where ammonium was a nitrogen source for nitrifying bacteria and diatoms.

Nitrate+nitrite were described in the water-column by

$$\frac{\partial NO_3}{\partial t} = Tr_t(dNO_3) + d\frac{N}{C}(\varepsilon_4 B_4 - \upsilon_1 P_1) \quad (16)$$

where nitrate was released by respiration of nitrifying bacteria and taken up by diatoms.

B.2.3. Phosphorus

The availability of phosphorus is generally considered in terms of orthophosphate. However, *Trichodesmium* exhibits high levels of alkaline phosphatase activity when inorganic P-stocks are minimal (Yentsch et al., 1972; Stihl et al., 2001). Concentrations of DOP and PO_4 are also enriched in and around blooms of *Trichodesmium* (Karl et al., 1992). During 1999, Lenes et al. (2001) measured increased surface DOP concentrations on the WFS at the onset of an offshore *Trichodesmium* bloom. When the population reached its maximum biomass (Fig. 6b), the water-column was devoid of both inorganic (Fig. 4b) and organic P stocks (Fig. 4b). Further model investigation of P dynamics suggested that available phosphorus was quickly assimilated by the diazotrophs during exponential growth phase, only to be released as organic P by excretion, grazing, and lysis (Lenes et al., 2005).

Therefore, the state equation for inorganic phosphorus (PO_4) was described by

$$\frac{\partial PO_4}{\partial t} = Tr_t(dPO_4) + d\frac{P}{C}(-\upsilon_n P_n + r_{3,4}\gamma_n P_n + \varepsilon_n P_n + \varepsilon_n B_n - \upsilon_4 B_4 + bDOP) \quad (17)$$

where phosphate was taken up by phytoplankton and nitrifying bacteria, and released during phytoplankton grazing, as well as by phytoplankton and both functional groups of bacteria during respiration.

The DOP state equation varies from that of DOC and DON due to *Trichodesmium*'s ability to utilize organic P for growth

$$\frac{\partial DOP}{\partial t} = Tr_t(dDOP) + d\frac{P}{C}(-\upsilon_2 P_2 + \psi_n P_n + (1 - r_{3,4})\gamma_n P_n + \chi_n P_n - \upsilon_3 B_3 + m_n B_n + k_d d_n + k_{fp} z_1 - bDOP) \quad (18)$$

where utilization by *Trichodesmium* and ammonifying bacteria were the major sinks.

B.2.4. Iron concentrations

Two pools of iron ($\mu mol\,Fe\,m^{-3}$) were incorporated into the model. The dissolved iron pool (dFe) was bioavailable to phytoplankton and nitrifying bacteria. The second pool, colloidal iron (cFe), represented an organically bound fraction, bioavailable to only the ammonifying bacteria. Since particulate inorganic iron is not bioavailable, it was ignored in the model. Rue and Bruland (1995, 1997) found that at low iron concentrations ($<0.6\,nmol\,kg^{-1}$) >99% of the dissolved iron was organically bound. Therefore, scavenging at lower concentrations is minimal (Johnson et al., 1997). This model incorporates a Michaelis–Menten-type kinetic relationship to calculate particle scavenging (α), similar to the work of Moore et al. (2002). They assumed a scavenging loss of 1% per year at iron concentrations below $0.6\,nmol\,kg^{-1}$, with increased scavenging as iron concentrations increased (maximum = 2.74% per day with a half-saturation of $2.5\,nmol\,kg^{-1}$). This accounted for increased particle reactivity as

dissolved iron concentrations exceed concentrations of organic ligands, and losses due to precipitation of iron oxides (Moore et al., 2002).

While their model focused on a global scale and multiyear period, our regional spatial scale and sub-yearly cases require faster scavenging to balance the photoreduction of colloidal iron as measured during DOTGOM III [Daughters of *Trichodesmium* in the Gulf of Mexico]. A maximum scavenging rate of 4.32% per day and half-saturation constant of 1.5 nmol dFe kg^{-1} was applied to [dFe] >0.3 nmol kg^{-1}. A higher minimum scavenging rate (0.432% per day) offset the daily light/dark cycling of dFe concentrations.

Photolytic reduction of colloidal iron by ultraviolet radiation has been shown to provide a mechanism for conversion of Fe(III) oxides and organically bound iron to the bioavailable dissolved pool (Wells et al., 1983; Wells and Mayer, 1991; Zhu et al., 1992; Johnson et al., 1994; Miller et al., 1995). It has been demonstrated that photoreduction of dissolved inorganic Fe(III) is not significant in waters with a pH above 6.5 (King et al., 1993). Therefore, Fe(III) photoreduction was attributed to organically complexed or colloidal iron (Miller et al., 1995).

Hong and Kester (1986) observed Fe(II) surface concentrations up to 12 nmol kg^{-1} off the coast of Peru with photoinduced variations. Similar concentrations ($\sim$15 nmol Fe kg^{-1}) were observed in Narragansett Bay (King et al., 1991). Miller (1990) reported diel variations in Fe(II) from Narragansett Bay of <0.2 to 1.5 nmol kg^{-1}. In July 2002 during DOTGOM III, O'Neil and Lenes (unpublished) measured diel variations of total dissolved Fe within offshore surface waters of <0.1–2.3 nmol kg^{-1}, with the rate of reduction and maximum concentration varying with the intensity of ultraviolet radiation, i.e. complete cloud cover on 11–12th of July and no cloud cover on 15th of July.

In the model, we attempt to account for diel fluctuations in the bioavailable iron pool by selecting a single "consumable" organic Fe(III) ligand pool (cFe) as a source for photoreduction (Miller et al., 1995). The equation to calculate the rate of photoreduction (k_{photo}) was after Johnson et al. (1994):

$$k_{photo} = \frac{k_{hvC}[cFe]I}{I_o} \tag{19}$$

where cFe was the concentration of colloidal iron and I, the irradiance. The maximum irradiance was $I_o = 2500\,\mu E\,m^{-2}\,s^{-1}$, and the rate constant $k_{hvC} = 2.33 \times 10^{-4}\,s^{-1}$. This equation ignores the wavelength dependence since only bulk rates are known.

The state equation for dissolved iron (dFe) was

$$\frac{\partial dFe}{\partial t} = Tr_t(\mathrm{d}dFe) + \mathrm{d}(-\upsilon_n P_n - \upsilon_n B_n - \alpha + k_{photo} + r_n\gamma_n P_n + \varepsilon_n P_n + \varepsilon_n B_n - xdfe) \tag{20}$$

where the four term (α) was particle scavenging. The fifth term, k_{photo}, was remineralization of colloidal iron to the dissolved pool by photolysis. The last term was a generic loss term for transfer to the higher trophic levels. The dissolved iron state equation was subject to iron input into the upper sigma level (dFe_i) based on wet (ϕ_1) and dry (ϕ_2) deposition of dust:

$$dFe_i = \frac{Fe_m Fe_d(\phi_1 + \phi_2)}{f} \tag{21}$$

where Fe_m (3.5%; Zhu et al., 1997) was the average mass fraction of iron in mineral rate of reduction and maximum concentration varying with the intensity of ultraviolet radiation, i.e. complete cloud cover on 11–12th of July and no cloud cover on 15th of July.

The state equation for colloidal iron (cFe) was

$$\frac{\partial cFe}{\partial t} = Tr_t(\mathrm{d}cFe) + \mathrm{d}\frac{\mathrm{Fe}}{\mathrm{C}}(-k_{photo} + \alpha + (1 - r_n)\gamma_n P_n + \chi_n P_n + \psi_n P_n + k_d d_n + k_{fp} z_1 - \upsilon_4 B_4 + m_n B_n) \tag{22}$$

where loss was due to photolysis and uptake by ammonifying bacteria (B_1). Phytoplankton and nitrifying bacteria used only dFe. Accumulation of colloidal iron was dependent upon the release of phytoplankton-bound iron during lysis (χ_n) and grazing, remineralization of detritus (k_d) and fecal pellets (k_{fp}), as well as excretion (ψ_n) by phytoplankton and bacterial mortality (m_n).

References

Barber, R.T., Chavez, F.P., 1991. Regulation of primary productivity rate in the equatorial Pacific. Limnology and Oceanography 36, 1803–1815.

Berman-Frank, I., Cullen, J.T., Shaked, Y., Sherrell, R.M., Falkowski, P.G., 2001. Iron availability, cellular iron quotas, and nitrogen fixation in *Trichodesmium*. Limnology and Oceanography 46 (6), 1249–1260.

Berman-Frank, I., Bidle, K.D., Haramity, L., Falkowski, P.G., 2004. The demise of the marine cyanobacterium, *Trichodesmium* spp., via an autocatalyzed cell death pathway. Limnology and Oceanography 49 (4), 997–1005.

Borstad, G.A., 1978. Some aspects of the occurrence and biology of *Trichodesmium* (Cyanophyta) in the Western Tropical Atlantic near Barbados, West Indies. Ph.D. Thesis, McGill University, Montreal, Canada, Unpublished.

Borstad, G.A., 1982. The influence of the meandering Guiana Current on the surface conditions near Barbados-temporal variations of *Trichodesmium* (Cyanophyta) and other plankton. Journal of Marine Research 40, 435–452.

Boyd, P.W., Watson, A.J., Law, C.S., Abraham, E.R., Trull, T., Murdoch, R., Bakker, D.C.E., Bowie, A.R., Buesseler, K.O., Chang, H., Charette, M., Croot, P., Downing, K., Frew, R., Gall, M., Hadfield, M., Hall, J., Harvey, M., Jameson, G., LaRoche, J., Liddicoat, M., Ling, R., Maldonado, M.T., McKay, R.M., Nodder, S., Pickmere, S., Pridmore, R., Rintoul, S., Safi, K., Sutton, P., Strzepek, R., Tanneberger, K., Turner, S., Waite, A., Zeldis, J., 2000. A mesoscale phytoplankton bloom in the polar Southern Ocean stimulated by iron fertilization. Nature 407 (6805), 695–702.

Broecker, W.S., 1982. Glacial to interglacial changes in ocean chemistry. Progress in Oceanography 11 (2), 151–197.

Caccia, V.G., Millero, F.J., 2003. The distribution and seasonal variation of dissolved trace metals in Florida Bay and adjacent waters. Aquatic Geochemistry 9 (2), 111–144.

Capone, D.G., Ferrier, M.D., Carpenter, E.J., 1994. Amino acid cycling in colonies of the planktonic marine cyanobacterium *Trichodesmium thiebautii*. Applied and Environmental Microbiology 60, 3989–3995.

Capone, D.G., Burns, J.A., Montoya, J.P., Subramaniam, A., Mahaffey, C., Gunderson, T., Michaels, A.F., Carpenter, E.J., 2005. Nitrogen fixation by *Trichodesmium* spp.: an important source of new nitrogen to the tropical and subtropical North Atlantic Ocean. Global Biogeochemical Cycles 19, GB2024.

Carder, K.L., Steward, R.G., Harvey, G.R., Ortner, P.B., 1989. Marine humic and fluvic acids: their effects on remote sensing of ocean chlorophyll. Limnology and Oceanography 34, 68–81.

Carder, K.L., Gregg, W.W., Costello, D.K., Haddad, K., Prospero, J.M., 1991. Determination of Saharan dust radiance and chlorophyll from CZCS imagery. Journal of Geophysical Research 96, 5369–5378.

Carpenter, E.J., 1983. Nitrogen fixation by marine *Oscillatoria* (*Trichodesmium*) in the world's oceans. In: Carpenter, E.J., Capone, D.G. (Eds.), Nitrogen in the Marine Environment. Academic Press, New York, pp. 65–103.

Carpenter, E.J., Price, C.C., 1977. Nitrogen fixation, distribution, and production of *Oscillatoria* (*Trichodesmium*) spp. in the western Sargasso and Caribbean seas. Limnology and Oceanography 22, 60–72.

Carpenter, E.J., Roman, K., 1991. Major role of the cyanobacterium *Trichodesmium* in nutrient cycling in the North Atlantic Ocean. Science 254 (5036), 1356–1358.

Carpenter, E.J., Roenneberg, T., 1995. The marine planktonic cyanobacteria *Trichodesmium* spp.: photosynthetic rate measurements in the SW Atlantic Ocean. Marine Ecology—Progress Series 118, 267–273.

Coale, K.H., Johnson, K.S., Fitzwater, S.E., Gordon, R.M., Tanner, S., Chavez, F.P., Ferioli, L., Sakamoto, C., Rogers, P., Millero, F., Steinberg, P., Nightingale, P., Cooper, D., Cochlan, W.P., Landry, M.R., Constantinou, J., Rollwagen, G., Trasvina, A., Kudela, R., 1996. A massive phytoplankton bloom induced by an ecosystem-scale iron fertilization experiment in the equatorial Pacific Ocean. Nature 383 (6600), 495–501.

del Giorgio, P.A., Cole, J.J., 2000. Bacterial growth energetics and growth efficiency. In: Kirchman, D.L. (Ed.), Microbial Ecology of the Oceans. Wiley-Liss, New York, NY, USA, pp. 289–325.

Devassy, V.P., Bhattathiri, P.M., Qasim, S.Z., 1978. *Trichodesmium* phenomena. Indian Journal of Marine Sciences 7, 168–186.

Dragovich, A., Kelly Jr., J.A., 1968. Hydrological and biological characteristics of Florida's west coast tributaries. Fisheries Bulletin 66 (3), 463–477.

Eppley, R.W., 1972. Temperature and phytoplankton growth in the sea. Fisheries Bulletin 70, 1063–1085.

Fennel, K., Spitz, Y.H., Letelier, R.M., Abbott, M.R., Karl, D.M., 2002. A deterministic model of N_2 fixation at stn. ALOHA in the subtropical North Pacific Ocean. Deep-Sea Research II 49, 149–174.

Froelich, P.N., Bender, M.L., Luedtke, N.A., Heath, G.R., Devries, T., 1982. The marine phosphorus cycle. American Journal of Science 282 (4), 474–511.

Glibert, P.M., Bronk, D.A., 1994. Release of dissolved organic nitrogen by marine diazotrophic cyanobacteria, *Trichodesmium* spp. Applied and Environmental Microbiology 60, 3996–4000.

Gregg, W.W., Carder, K.L., 1990. A simple spectral solar irradiance model for cloudless maritime atmospheres. Limnology and Oceanography 35 (8), 1657–1675.

Gordon, H.R., Brown, O.B., Evans, R.H., Brown, J.W., Smith, R.C., Baker, K.S., Clark, D.K., 1988. A semianalytical radiance model of ocean color. Journal of Geophysical Research 93, 10,909–10,924.

Gordon, R.M., Johnson, K.S., Coale, K.H., 1998. The behaviour of iron and other trace elements during the IronEx-I and PlumEx experiments in the Equatorial Pacific. Deep-Sea Research II 45 (6), 995–1041.

He, R.Y., Weisberg, R.H., 2002a. West Florida Shelf circulation and temperature budget for the 1999 spring transition. Continental Shelf Research 22, 719–748.

He, R.Y., Weisberg, R.H., 2002b. Tides on the West Florida Shelf. Journal of Physical Oceanography 32 (12), 3455–3473.

He, R., Weisberg, R.H., 2003. A loop current intrusion case study on the west Florida Shelf. Journal of Physical Oceanography 33 (2), 465–477.

Hewson, I., Govil, S.R., Capone, D.G., Carpenter, E.J., Furman, J.A., 2004. Evidence of *Trichodesmium* viral lysis and potential significance for biogeochemical cycling in the oligotrophic ocean. Aquatic Microbial Ecology 36, 1–8.

Hong, H.S., Kester, D.R., 1986. Redox state of iron in the offshore waters of Peru. Limnology and Oceanography 31 (3), 512–524.

Hood, R.R., Bates, N.R., Capone, D.G., Olson, D.B., 2001. Modeling the effect of nitrogen fixation on carbon and nitrogen fluxes at BATS. Deep-Sea Research II 48, 1609–1648.

Hood, R.R., Coles, V.J., Capone, D.G., 2004. Modeling the distribution of *Trichodesmium* and nitrogen fixation in the Atlantic Ocean. Journal of Geophysical Research 109, C06006.

Johnson, K.S., Coale, K.H., Elrod, V.A., Tindale, N.W., 1994. Iron photochemistry in seawater from the equatorial Pacific. Marine Chemistry 46 (4), 319–334.

Johnson, K.S., Gordon, R.M., Coale, K.H., 1997. What controls dissolved iron concentrations in the world ocean? Marine Chemistry 57, 137–161.

Karl, D.M., Letelier, R., Hebel, D.V., Bird, D.F., Winn, C.D., 1992. *Trichodesmium* blooms and new nitrogen in the North Pacific Gyre. In: Carpenter, E.J., Capone, D.A., Rueter, J.G. (Eds.), Marine Pelagic Cyanobacteria: *Trichodesmium* and other Diazotrophs. Kluwer Academic Publishers, Netherlands, pp. 219–237.

Karl, D.M., Letelier, R., Tupas, L., Dore, J., Christian, J., Hebel, D., 1997. The role of nitrogen fixation in biogeochemical cycling in the subtropical North Pacific Ocean. Nature 388, 533–538.

Kim, Y.S., Martin, D.F., 1974. Interrelationship of Peace River parameters as a basis of the iron index: a predictive guide to the Florida red tide. Water Research 8, 607–616.

King, J.E., 1950. A preliminary report on the plankton of the west coast of Florida. Quarterly Journal of Florida Academy of Sciences 12, 109–137.

King, D.W., Lin, J., Kester, D.R., 1991. Determination of Fe(II) in seawater at nanomolar concentrations. Analytica Chimica Acta 247, 125–132.

King, D.W., Aldrich, R.A., Charnecki, S.E., 1993. Photochemical redox cycling of iron in NaCl solutions. Marine Chemistry 44, 105–120.

Kirk, J.T.O., 1994. Light and Photosynthesis in Aquatic Systems. Cambridge University Press, Cambridge, 509pp.

Kromkamp, J., Walsby, A.E., 1992. Buoyancy regulation and vertical migration of *Trichodesmium*: a computer model prediction. In: Carpenter, E.J., Capone, D.A., Rueter, J.G. (Eds.), Marine Pelagic Cyanobacteria: *Trichodesmium* and other diazotrophs. Kluwer Academic Publishers, Netherlands, pp. 239–248.

Landing, W.M., Perry, J.J., Guentzel, J.L., Gill, G.A., Pollman, C.D., 1995. Relationships between the atmospheric deposition of trace elements, major ions, and mercury in Florida: the FAMS project (1992–1993). Water, Air, and Soil Pollution 80, 343–352.

Lenes, J.M., 2002. Iron fertilization of *Trichodesmium* off the west coast of Barbados: a one-dimensional numerical model. Master's Thesis, University of South Florida, St. Petersburg, FL.

Lenes, J.M., 2006. Saharan dust and phosphatic fidelity: a three dimensional biogeochemical model of *Trichodesmium* on the West Florida shelf. Ph.D. Dissertation, University of South Florida, Tampa.

Lenes, J.M., Darrow, B.P., Cattrall, C., Heil, C.A., Callahan, M., Vargo, G.A., Byrne, R.H., Prospero, J.M., Bates, D.E., Fanning, K.A., Walsh, J.J., 2001. Iron fertilization and the *Trichodesmium* response on the West Florida Shelf. Limnology and Oceanography 46 (6), 1261–1277.

Lenes, J.M., Walsh, J.J., Otis, D.B., Carder, K.L., 2005. Iron fertilization of *Trichodesmium* off the west coast of Barbados: a one-dimensional numerical model. Deep-Sea Research I 52, 1021–1041.

Lester, K.M., Merkt, R., Heil, C.A., Vargo, G.A., Neely, M.B., Spence, D.N., Melahn, L., Walsh, J.J., 2001. Evolution of a *Gymnodinium breve* (Gymnodiniales, Dinophyceae) red tide on the West Florida Shelf: relationship with organic N and P. In: Hallegraeff, G.H., Blackburn, S.I., Bolch, C.J., Lewis, R.J. (Eds.), Harmful Algal Blooms. Hobart, Australia, pp. 161–164.

Martin, J.H., Fitzwater, S.E., 1988. Iron deficiency limits phytoplankton growth in the northeast Pacific subarctic. Nature 331, 341–343.

Martin, J.H., Gordon, R.M., Fitzwater, S.E., 1991. The case for iron. Limnology and Oceanography 36 (8), 1793–1802.

Masserini, R.T., Fanning, K.A., 2000. A sensor package for the simultaneous determination of nanomolar concentrations of nitrite, nitrate, and ammonia in seawater by fluorescence detection. Marine Chemistry 68 (4), 323–333.

McCarthy, J.J., Carpenter, E.J., 1979. *Oscillatoria* (*Trichodesmium*) *thiebautii* (Cyanophyta) in the central North Atlantic Ocean. Journal of Phycology 15, 75–82.

Mellor, G.L., Yamada, T., 1982. Development of a turbulence closure model for geophysical fluid problems. Review of Geophysical Space Physics 20, 851–875.

Miller, W.L., 1990. An investigation of peroxide, iron, and iron bioavailability in irradiated marine waters. Ph.D. Thesis, University of Rhode Island, Kingston, RI, 400pp.

Miller, W.L., King, D.W., Lin, J., Kester, D.R., 1995. Photochemical redox cycling of iron in coastal waters. Marine Chemistry 50, 63–77.

Mills, M.M., Ridame, C., Davey, M., LaRoche, J., Geider, R.J., 2004. Iron and phosphorus co-limit nitrogen fixation in the eastern tropical North Atlantic. Nature 429, 292–294.

Moore, J.K., Doney, S.C., Kleypas, J.A., Glover, D.M., Fung, I.Y., 2002. An intermediate complexity marine ecosystem model for the global domain. Deep-Sea Research II 49, 403–462.

Morel, A., Ahn, Y.-H., 1990. Optical efficiency of free-living marine bacteria: influence of bacterioplankton upon the optical properties and particulate organic carbon in oceanic waters. Journal of Marine Research 48, 145–175.

Muhs, D.R., Budahn, J., Prospero, J.M., Carey, S.N., 2007. Geochemical evidence for African dust inputs to soils of western Atlantic islands: Barbados, the Bahamas, and Florida. Journal of Geophysical Research 112, D13203.

Mulholland, M.R., Capone, D.G., 2000. The nitrogen physiology of the marine N_2-fixing cyanobacteria *Trichodesmium* spp. Trends in Plant Science 5, 148–153.

Mulholland, M.R., Ohki, K., Capone, D.G., 2001. Nutrient controls on nitrogen uptake and metabolism by natural populations and cultures of *Trichodesmium* (Cyanobacteria). Journal of Phycology 37, 1001–1009.

Mulholland, M.R., Heil, C.A., Bronk, D.A., O'Neil, J.M., Bernhardt, P.W., 2004. Does nitrogen regeneration from N_2 fixing cyanobacteria *Trichodesmium* spp. fuel *Karenia* blooms in the Gulf of Mexico. In: Steidinger, K.A., Landsberg, J.H., Tomas, C.R., Vargo, G.A. (Eds.), Harmful Algae 2002. Florida Fish and Wildlife Conservation Commission, Florida Institute of Oceanography, and Intergovernmental Oceanographic Commission of UNESCO, pp. 47–49.

Mulholland, M.R., Bernhardt, P.W., Heil, C.A., Bronk, D.A., O'Neil, J.M., 2006. Nitrogen fixation and release of fixed nitrogen by Trichodesmium spp. in the Gulf of Mexico. Limnology and Oceanography 51, 1762–1776.

Mullin, M.M., Stewart, E.F., Fuglister, F.J., 1975. Ingestion by planktonic grazers as a function of concentration of food. Limnology and Oceanography 20, 259–262.

Nelson, J.R., Robertson, C.Y., 1993. Detrital spectral absorption: laboratory studies of visible light effects on phytodetritus absorption, bacterial spectral signal, and comparison to field measurements. Journal of Marine Research 51, 181–207.

O'Neil, J.M., Roman, M.R., 1992. Grazers and associated organisms of *Trichodesmium*. In: Carpenter, E.J., Capone, D.A., Rueter, J.G. (Eds.), Marine Pelagic Cyanobacteria: *Trichodesmium* and other Diazotrophs. Kluwer Academic Publishers, Netherlands, pp. 239–248.

Orcutt, K.M., Lipschultz, F.J., Gundersen, K., Arimoto, R., Michaels, A.F., Knap, A.H., Gallon, J.R., 2001. A seasonal study of the significance of N_2 fixation by *Trichodesmium* at the Bermuda Atlantic Time-series (BATS) site. Deep-Sea Research II 48, 1583–1608.

Peng, T.H., Takahashi, T., Broecker, W.S., Olafsson, J., 1987. Seasonal variability of carbon dioxide, nutrients and oxygen in the northern North Atlantic surface water: observations and a model. Tellus, Series B 39, 439–458.

Pope, R.M., Fry, E.S., 1997. Absorption spectrum (380–700 nm) of pure water. 2. Integrating cavity measurements. Applied Optics 36 (33), 8710–8723.

Proctor, L.M., Fuhrman, J.A., 1990. Viral mortality of marine bacteria and cyanobacteria. Nature 343, 60–62.

Proctor, L.M., Fuhrman, J.A., 1991. Roles of viral-infection in organic particle-flux. Marine Ecology—Progress Series 69 (1–2), 133–142.

Prospero, J.M., 1999a. Long-range transport of mineral dust in the global atmosphere: impact of African dust on the environment of the southeastern United States. Proceedings of the National Academy of Sciences USA 96 (7), 3396–3403.

Prospero, J.M., 1999b. Long-term measurement of the transport of African mineral dust to the southeastern United States: implications for regional air quality. Journal of Geophysical Research 104, 15,917–15,927.

Prospero, J.M., Lamb, P.J., 2003. African droughts and dust transport to the Caribbean: climate change implications. Science 302, 1024–1027.

Prospero, J.M., Nees, R.T., Uematsu, M., 1987. Deposition rate of particulate and dissolved aluminum derived from Saharan dust in precipitation at Miami, Florida. Journal of Geophysical Research 92, 14,723–14,731.

Prospero, J.M., Olmez, I., Ames, M., 2001. Al and Fe in PM2.5 and PM10 suspended particles in south-central Florida: the impact of long-range transport of African mineral dust. Water, Air, and Soil Pollution 125 (1–4), 291–317.

Prufert-Bebout, L., Paerl, H.W., Lassen, C., 1993. Growth, nitrogen-fixation, and spectral attenuation in cultivated *Trichodesmium* species. Applied and Environmental Microbiology 59, 1367–1375.

Ridame, C., Guieu, C., 2002. Saharan input of phosphate to the oligotrophic water of the open western Mediterranean Sea. Limnology and Oceanography 47 (3), 856–869.

Roesler, C.S., Perry, M.J., Carder, K.L., 1989. Modeling in situ phytoplankton absorption from total absorption spectra in productive inland marine waters. Limnology and Oceanography 34 (8), 1510–1523.

Rue, E.L., Bruland, K.W., 1995. Complexation of iron(III) by natural organic-ligands in the central north Pacific as determined by a new competitive ligand equilibration adsorptive cathodic stripping voltammetric method. Marine Chemistry 50 (1–4), 117–138.

Rue, E.L., Bruland, K.W., 1997. The role of organic complexation on ambient iron chemistry in the equatorial Pacific Ocean and the response of a mesoscale iron addition experiment. Limnology and Oceanography 42 (5), 901–910.

Sanudo-Wilhelmy, S.A., Kustka, A.B., Gobler, C.J., Hutchins, D.A., Yang, M., Lwiza, K., Burns, J., Capone, D.G., Carpenter, E.J., 2001. Phosphorus limitation of nitrogen fixation by *Trichodesmium* in the central Atlantic Ocean. Nature 411, 66–69.

Sellner, K.G., 1997. Physiology, ecology, and toxic properties of marine cyanobacteria blooms. Limnology and Oceanography 42, 1089–1104.

Sheridan, C.C., Steinberg, D.K., Kling, G.W., 2002. The microbial and metazoan community associated with colonies of *Trichodesmium* spp.: a quantitative survey. Journal of Plankton Research 24, 913–922.

Smith, R.C., Baker, K.S., 1981. Optical properties of the clearest natural waters (200–800 nm). Applied Optics 20, 177–184.

Steidinger, K.A., Vargo, G.A., Tester, P.A., Tomas, C.R., 1998. Bloom dynamics and physiology of *Gymnodinium breve* with emphasis on the Gulf of Mexico. In: Anderson, D.M., Cembella, A.D., Hallegraeff, G.H. (Eds.), Physiological Ecology of Harmful Algal Blooms. Springer, Berlin, pp. 135–153.

Stihl, A., Sommer, U., Post, A.F., 2001. Alkaline phosphatase activities among populations of the colony-forming diazotrophic cyanobacterium *Trichodesmium* spp. (cyanobacteria) in the Red Sea. Journal of Phycology 37 (2), 310–317.

Subramaniam, A., Carpenter, E.J., Falkowski, P.G., 1999. Bio-optical properties of the marine diazotrophic cyanobacteria *Trichodesmium* spp. I. A reflectance model for remote sensing. Limnology and Oceanography 44, 618–627.

Tegen, I., Fung, I., 1994. Modeling of mineral dust in the atmosphere–Sources, transport, and optical thickness. Journal of Geophysical Research 99 (D11), 22,897–22,914.

Turner, J.T., Rabalais, N.R., 1994. Coastal eutrophication near the Mississippi river delta. Nature 368, 619–621.

U.S.G.S., 1976–1981. Water Resources Data for Florida. US Geological Survey Water Data Reports.

Vargo, G.A., Carder, K.L., Gregg, W., Shanley, E., Heil, C., Steidinger, K.A., Haddad, K., 1987. The potential contribution of primary production of red tides to the West Florida Shelf ecosystem. Limnology and Oceanography 32 (3), 762–767.

Villareal, T.A., Carpenter, E.J., 1990. Diel buoyancy regulation in the marine diazotrophic cyanobacterium *Trichodesmium thiebautii*. Limnology and Oceanography 35, 1832–1837.

Walsby, A.E., 1978. The properties and buoyancy providing role of gas vesicles in *Trichodesmium ehrenberg*. British Phycological Journal 12, 103–116.

Walsby, A.E., 1992. The gas vesicles and buoyancy of *Trichodesmium*. In: Carpenter, E.J., Capone, D.A., Rueter, J.G. (Eds.), Marine Pelagic Cyanobacteria: *Trichodesmium* and other Diazotrophs. Kluwer Academic Publishers, Netherlands, pp. 141–161.

Walsh, J.J., Steidinger, K.A., 2001. Saharan dust and Florida red tides: the cyanophyte connection. Journal of Geophysical Research—Oceans 106, 11,597–11,612.

Walsh, J.J., Weisberg, R.H., Dieterle, D.A., He, R., Darrow, B.P., Jolliff, J.K., Lester, K.M., Vargo, G.A., Kirkpatrick, G.J., Fanning, K.A., Sutton, T.T., Jochens, A.E., Biggs, D.C., Nababan, B., Hu, C., Muller-Karger, F.E., 2003. A phytoplankton response to intrusions of slope water on the West Florida Shelf: models and observations. Journal of Geophysical Research 108, 3190.

Walsh, J.J., Jolliff, J.K., Darrow, B.P., Lenes, J.M., Milroy, S.P., Dieterle, D.A., Carder, K.L., Chen, F.R., Vargo, G.A., Weisberg, R.H., Fanning, K.A., Muller-Karger, F.E., Steidinger, K.A., Heil, C.A., Tomas, C.R., Prospero, J.S., Lee, T.N., Kirkpartick, G.J., Whitledge, T.E., Stockwell, D.A., Villareal, T.A., Jochens, A.E., Bontempi, P.S., 2006. Red tides: where, when, why? Journal of Geophysical Research, 111, C11003, doi:10.1029/2004JC002813.

Weisberg, R.H., He, R., 2003. Local and deep-ocean forcing contributions to anomalous water properties on the West Florida Shelf. Journal of Geophysical Research 108 (C6), 3184.

Weiss, R.F., 1970. The solubility of nitrogen, oxygen and argon in water and seawater. Deep-Sea Research 17, 721–735.

Wells, M.L., Mayer, L.M., 1991. The photoconversion of colloidal iron oxyhydroxides in seawater. Deep-Sea Research 38, 1379–1395.

Wells, M.L., Zorkin, N.G., Lewis, A.G., 1983. The role of colloidal chemistry in providing a source of iron to phytoplankton. Journal of Marine Research 41, 731–746.

Yentsch, C.M., Yentsch, C.S., Perras, J.P., 1972. Alkaline phosphatase activity in the tropical marine blue-green alga *Oscillatoria erythaea* ("*Trichodesmium*"). Limnology and Oceanography 17, 772–774.

Zhu, X.R., Prospero, J.M., Millero, F.J., Savoie, D.L., Brass, G.W., 1992. The solubility of ferric ion in marine mineral aerosol solutions at ambient relative humidities. Marine Chemistry 38, 91–107.

Zhu, X.R., Prospero, J.M., Millero, F.J., 1997. Diel variability of soluble Fe(II) and soluble total Fe in North African dust in the trade winds at Barbados. Journal of Geophysical Research 102, 21,297–21,306.